Data clustering for classification of vegetable biomass from compositional data

A tool for biomass valorization

Durán-Aranguren, Daniel D.; Toro-Delgado, Juan; Núñez-Barrero, Valentina; Florez-Bulla, Valentina; Sierra, Rocío; Posada, John A.; Mussatto, Solange I.

DOI
10.1016/j.biombioe.2024.107447

Publication date
2024

Document Version
Final published version

Published in
Biomass and Bioenergy

Citation (APA)
Durán-Aranguren, D. D., Toro-Delgado, J., Núñez-Barrero, V., Florez-Bulla, V., Sierra, R., Posada, J. A., & Mussatto, S. I. (2024). Data clustering for classification of vegetable biomass from compositional data: A tool for biomass valorization. *Biomass and Bioenergy*, *191*, Article 107447. https://doi.org/10.1016/j.biombioe.2024.107447

Biomass and Bioenergy 191 (2024) 107435

Contents lists available at ScienceDirect

Biomass and Bioenergy

journal homepage: www.elsevier.com/locate/biombioe

Integrated kinetic modeling of acetone-butanol-ethanol fermentation by *Clostridium saccharoperbutilacetonicum* N1-4: Co-utilization strategy with cane molasses, biomass-derived sugars, and furaldehydes

Roger Assis de Oliveira [a], Ana Maria Zetty Arenas [b,c,d], José Plácido [a], Laura Plazas Tovar [a,*]

[a] Department of Chemical Engineering, Federal University of São Paulo, ZIP code 09913-030, Diadema, São Paulo, Brazil
[b] School of Chemical Engineering, University of Campinas, ZIP code 13083-852, Campinas, São Paulo, Brazil
[c] Department of Biotechnology, Delft University of Technology, ZIP code 13083-852, Delft, the Netherlands
[d] Brazilian Biorenewables National Laboratory (LNBR), Brazilian Center for Research in Energy and Materials (CNPEM), ZIP code: 13083-970, Campinas, São Paulo, Brazil

ARTICLE INFO

Keywords:
ABE fermentation
Biobutanol
Furan derivatives
Kinetic modeling
Lignocellulosic biomass
Parameter optimization

ABSTRACT

Sugar-based byproducts such as molasses and bagasse are abundant resources for large-scale biobutanol commercialization. This study presents a comprehensive kinetic model to analyze ABE (acetone-butanol-ethanol) fermentation by *C. saccharoperbutilacetonicum N1-4*, emphasizing diverse carbon sources and furaldehyde co-utilization. By leveraging sensitivity analysis against models in the literature and the proposed model as well as parameter optimization using *Scilab*®, the potential for the simultaneous utilization of sugarcane molasses and bagasse-derived sugars alongside furfural and HMF for butanol synthesis was assessed. These findings revealed that despite the microbial preference for hexose sugars, the incorporation of up to 25% pentose sugars did not significantly hinder butanol production. However, furaldehydes perturbed butyric acid assimilation and acetyl-CoA consumption while enhancing acetone-butanol-ethanol synthesis. The simulation highlighted the peak concentrations of furfural and HMF (0.33 mmol L^{-1} and 0.03 mmol L^{-1}, respectively), underscoring their conversion to less toxic alcohols, thereby augmenting metabolism. Sensitivity analysis underscores the necessity of enhancing butyric acid assimilation, providing critical insights for optimizing ABE fermentation and advancing biobutanol production from sugar-based byproducts.

1. Introduction

The transition towards a cost-effective, non-food-based, and reliably available feedstock on an industrial scale is crucial for considering biobutanol as a versatile chemical and feedstock for sustainable aviation fuel production [1]. Despite the projected production rates of 107 million liters of bioalcohols in 2022 and 142 billion liters of biodiesel by 2023 [2], biobutanol production via acetone-butanol-ethanol (ABE) fermentation has faced several large-scale production and commercialization problems due to the low yield and productivity of the final product resulting from the toxicity of the fermentation broth to most *Clostridium* strains, such as *Clostridium acetobutylicum* [3], *Clostridium beijerinckii* [4], *Clostridium saccharobutylicum* [5], and *Clostridium saccharoperbutylicum* [6]. Additionally, the utilization of high-cost feedstocks, such as starch [7], mono-, di-, and polysaccharides [8,9], presents significant challenges.

Low-cost and non-food carbon sources such as lignocellulosic materials are significantly more economical than other available options [10]. Depolymerization methods applied to lignocellulosic biomass can produce a mixture of sugars, aromatic monomers, and furaldehydes, which varies depending on the specific type of biomass used. Understanding the cellular physiology during the simultaneous utilization of mixed substrates as carbon sources is particularly interesting. The *Clostridium* strain can utilize various types of hexoses and pentoses as carbon sources [8]; however, it has limitations and cannot consume them simultaneously because of its dominant preference for glucose. As a result, metabolic pathways for less-preferred sugars such as xylose were identified as being inactivated [6,11]. This hinders efficient utilization of lignocellulosic biomass in the continuous production of biobutanol and negatively affects the economics of the fermentation

* Corresponding author.
E-mail address: laura.tovar@unifesp.br (L.P. Tovar).

https://doi.org/10.1016/j.biombioe.2024.107435
Received 25 June 2024; Received in revised form 25 September 2024; Accepted 12 October 2024
Available online 22 October 2024

process.

Gene regulation enhances the co-utilization of sugars and furaldehydes and increases solvent tolerance [12]. However, this technique alone is insufficient for commercial ABE fermentation [13]. A phenomenological model that combines experimental efforts with characterization of fermentation metabolism can be used in bottleneck analysis and process optimization, and its development is crucial to address the challenges of biorefineries based on the use of sugar biomass and furaldehydes. Such a model would enable the identification of limitations such as the low growth rate of microorganisms, low solvent tolerance, low titer and productivity of butanol, and the alternative use of biorefinery substrates [14,15].

ABE fermentation models can be categorized based on the hypotheses about the metabolic pathways they propose. A collection of 15 structured models, detailed in the Supplementary Material (S-1), examines the metabolic pathways of various cell types and the impact of reactions and metabolic intermediates on the process. Specifically, the structured models reported in Table 1 include those that use individual sugars, such as glucose [16–18] or xylose [19–21]. Raganati et al. [22] expanded on the studies by Shinto et al. [16] and Shinto et al. [19] to include a wide variety of sugars, such as pentoses (xylose and arabinose), hexoses (glucose, fructose, and mannose), and disaccharides (sucrose and lactose). However, each sugar has been studied separately. Díaz and Willis [11] were the first to develop a structured model for mixed sugars (glucose and xylose); however, they still deal with reagents of analytical purity. Birgen et al. [23], Lim et al. [24], Lim et al. [25] and Rivas-Astroza et al. [4] presented unstructured models for the fermentation of a mixture of glucose and xylose. Liao et al. [26] pioneered the simultaneous consideration of the effects of extracellular environment, metabolism, and genetic regulation on this process.

These models often simplify the complex interactions between diverse substrates and metabolic pathways, overlooking the competitive and inhibitory effects observed in mixed-substrate fermentations. Despite these advancements, existing kinetic models inadequately capture the dynamics of ABE fermentation when co-utilizing biomass-derived sugar (such as hexoses and pentoses) and furaldehydes (such as furfural and 5-hydroxymethyl furfural or HMF), which are typically formed during hemicellulose hydrolysis, leading to suboptimal process optimization and scale-up. This work developed a dynamic kinetic model that encompasses the simultaneous fermentation of multiple carbon sources: glucose, fructose, sucrose, xylose, and arabinose. It also evaluates the effects of various compounds on cell growth. Model I examines the impact of butanol concentration alone, Model II considers the effects of both butanol and furaldehydes, and Model III includes butanol, furaldehydes, acetic acid, and butyric acid.

Real data from batch fermentation consisting of molasses and residual hemicellulosic hydrolysate, described by Zetty-Arenas et al. [6], were used to estimate the model parameters and extensive sensitivity analysis was performed using *Scilab*® to identify the critical parameters affecting the final butanol concentration. Through dynamic kinetic modeling and sensitivity analysis, we explored the interactions between multiple carbon sources and fermentation by-products. Our findings reveal novel insights into optimizing substrate co-utilization, paving the way for more efficient biobutanol production processes.

2. Materials and methods

2.1. Microorganism, data, and calculation of specific rates

Fermentation data for the *Clostridium saccharoperbutylacetonicum DSM 14923(N1-4)* strain published by Zetty-Arenas et al. [6] containing time profiles (from 0 to 72 h) of concentration ($g.L^{-1}$) of monosaccharides (arabinose, xylose, glucose, and fructose), disaccharide (sucrose), organic acids (acetic acid and butyric acid), ABE (acetone, butanol, and ethanol) and furan derivatives (furfural and HMF) were used to model the carbon sources and furaldehydes intake, cellular growth, and ABE production kinetics. The data for the kinetic modeling were derived from batch co-utilization of raw sugarcane molasses and hemicellulosic hydrolysate, which was conducted in DASGIP Model Box 300 mL bioreactors (Eppendorf, Hamburg, Germany) with working volumes of 240 mL. The reactions were allowed to proceed for 72 h at 30 °C, and the pH was adjusted to 7.0 using 25 % (w/w%) NH_4OH aqueous solution. The medium contained approximately 30 g L^{-1} of carbon source supplemented with a modified sterile P2, the original medium reported by Qureshi and Blaschek [27] and modified by Zetty-Arenas et al. [28] and Zetty-Arenas et al. [6].

In this study three sugar-fermentation carbon sources, from cane molasses and biomass-derived sugars, were selected as follows:

- Pure molasses (~30 g L^{-1}), hereafter referred to as **M100**, with experimental data reported by Zetty-Arenas et al. [6].
- Mixture consisting of 75 % sugars from molasses (22.5 g L^{-1}) and 25 % sugars from crude hemicellulose hydrolysate (7.5 g L^{-1}), herein referred to as **M75HH25**, with experimental data reported in this work.
- Mixture consisting of 75 % sugars from molasses (22.5 g L^{-1}) and 25 % sugars from detoxified concentrate hemicellulose hydrolysate (7.5 g L^{-1}), herein referred to as **M75CHH25**), with experimental data reported by Zetty-Arenas et al. [6].

Considering the carbon source (*Sur*: glucose, fructose, sucrose, xylose, and arabinose) and solvent (*Sol*: acetone, butanol, and ethanol) concentrations ($g.L^{-1}$) at one fermentation time (t_1) and immediately following (t_2), then the specific rates of carbon source consumption (q_s: $g.gdw^{-1}.h^{-1}$ – where "gdw" means grams of cells in dry weight), growth rate (μ: h^{-1}), and ABE production rate (q_p: $g.gdw^{-1}.h^{-1}$) were calculated using **Equations (1)–(3).**

$$q_s = \left(\frac{Sur_{t1} - Sur_{t2}}{t_2 - t_1}\right)\left[\frac{1}{\left(\frac{Cell_{t1}+Cell_{t2}}{2}\right)}\right] \quad (1)$$

$$\mu = \left(\frac{Cell_{t1} - Cell_{t2}}{t_2 - t_1}\right)\left[\frac{1}{\left(\frac{Cell_{t1}+Cell_{t2}}{2}\right)}\right] \quad (2)$$

$$q_p = \left(\frac{Sol_{t2} - Sol_{t1}}{t_2 - t_1}\right)\left[\frac{1}{\left(\frac{Cell_{t1}+Cell_{t2}}{2}\right)}\right] \quad (3)$$

2.2. Sensitivity, robustness, and identifiability in published kinetics models

The structured models of Shinto et al. [16] and Shinto et al. [19] were used to analyze the most influential parameters in the fermentation of individual sugars. The model proposed by Shinto et al. [16] evaluated only the glucose consumption and presented 19 reactions and 45 parameters (Table 1). In addition, the dynamic kinetic model reported by Shtino et al. [19] was used to evaluate xylose consumption using 25 reactions and 57 parameters (Table 1). For the sensitivity analysis of fructose and sucrose, the Shinto et al. [16] metabolic pathway was utilized, along with parameter values as documented by Raganati et al. [22].

The parameters analyzed using parametric sensitivity are presented in Fig. 1a and Table 2. In addition, the parameter values varied with different factors (Fig. 1a) around the base values reported by Shinto et al. [16] and Shinto et al. [19].

The sensitivity, as proposed by Shinto et al. [16], was determined according to the deviation in the final concentration of butanol (*ED*, **Equation (4)**) and the deviation between the mean areas of the temporal profiles of the butanol concentration (integral deviation or *ID*,

Table 1
Chemical reactions considered (✔) in the metabolic pathways for ABE fermentation by several structured models.

Reaction	[a]	[b]	[c]	[d]	[e]	[f]	[g]	[h]	[i]	[j]	This work
Glucose → Fructose 6-P	✖	✔	✔	✔	✔	✔	✖	✖	✔	✖	✔
Xylose → Fructose 6-P	✖	✖	✖	✖	✖	✖	✖	✖	✖	✔	✖
Mannose → Fructose 6-P	✖	✖	✖	✔	✖	✖	✖	✖	✖	✖	✖
Sucrose → 2 Fructose 6-P	✖	✖	✖	✔	✖	✖	✖	✖	✖	✖	✖
Lactose → Fructose 6-P + 2 Glyceraldehyde 3-P	✖	✖	✖	✔	✖	✖	✖	✖	✖	✖	✖
Fructose 6-P → Glyceraldehyde 3-P	✖	✔	✔	✔	✔	✔	✖	✔	✔	✔	✔
Sucrose → Sucrose 6-P	✖	✖	✖	✖	✖	✖	✖	✖	✖	✖	✔
Sucrose 6-P → Fructose 6-P	✖	✖	✖	✖	✖	✖	✖	✖	✖	✖	✔
Fructose → Fructose 6-P	✖	✖	✖	✔	✖	✖	✖	✖	✖	✖	✔
Glyceraldehyde 3-P → Pyruvate	✖	✔	✔	✔	✔	✔	✖	✔	✔	✔	✔
Lactate → Pyruvate	✖	✔	✔	✖	✔	✔	✖	✔	✔	✔	✔
Pyruvate → Lactate	✖	✔	✔	✖	✔	✔	✖	✔	✔	✔	✔
Pyruvate → Acetyl-CoA+ $2CO_2$	✔	✔	✔	✔	✔	✔	✔	✔	✔	✔	✔
Acetate → Acetyl-P→ Acetyl-CoA	✖	✔	✔	✔	✖	✔	✔	✔	✔	✔	✔
Acetate + Acetoacetyl-CoA→ Acetoacetate + Acetyl-CoA	✔	✔	✔	✖	✔	✔	✖	✖	✖	✔	✔
Acetoacetate + Acetyl-CoA→ Acetate + Acetoacetyl-CoA	✔	✖	✖	✖	✖	✖	✖	✖	✖	✖	✖
Acetyl-CoA→ Acetyl-P → Acetate	✖	✔	✔	✖	✖	✔	✖	✖	✖	✔	✔
Acetyl-CoA→ Acetate	✔	✖	✖	✔	✔	✖	✔	✔	✔	✖	✖
Acetyl-CoA→ Acetoacetyl-CoA + CoA	✔	✔	✔	✔	✔	✔	✔	✔	✔	✔	✔
Acetyl-CoA→ Acetaldehyde → Ethanol	✖	✔	✔	✖	✖	✔	✖	✖	✖	✔	✔
Acetyl-CoA→ Ethanol	✔	✖	✖	✔	✔	✖	✔	✔	✔	✖	✖
Acetyl-CoA→ Cells	✖	✔	✔	✔	✖	✔	✖	✔	✔	✔	✖
Cells → Inactive Cells	✖	✔	✔	✔	✔	✔	✖	✔	✔	✔	✖
Acetoacetyl-CoA→Butyryl-CoA	✖	✔	✔	✔	✔	✔	✔	✔	✔	✔	✔
Butyrate + Acetoacetyl-CoA→ Acetoacetate + Butyryl-CoA	✖	✔	✔	✖	✔	✔	✖	✖	✖	✔	✔
Acetoacetate → Acetone + CO_2	✔	✔	✔	✖	✔	✔	✖	✖	✖	✔	✔
Butyrate →Butyryl-P →Butyryl-CoA	✖	✔	✔	✖	✖	✔	✖	✖	✖	✔	✔
Butyrate →Butyryl-CoA	✔	✖	✖	✔	✖	✖	✔	✔	✔	✖	✖
Butyryl-CoA →Butyryl-P → Butyrate	✖	✔	✔	✖	✖	✔	✖	✖	✖	✔	✔
Butyryl-CoA →Butyrate	✖	✖	✖	✔	✔	✖	✔	✔	✔	✖	✖
Butyryl-CoA → Butyryladehyde → Butanol	✖	✔	✔	✖	✖	✔	✖	✖	✖	✔	✔
Butyryl-CoA → Butanol	✔	✖	✖	✔	✔	✖	✔	✔	✔	✖	✖
Xylose → Xylulose 5-P	✖	✖	✔	✔	✖	✖	✖	✔	✖	✖	✔
Arabinose → Xylulose 5-P	✖	✖	✖	✔	✖	✖	✖	✖	✖	✖	✖
Arabinose → Ribose 5-P	✖	✖	✖	✖	✖	✖	✖	✖	✖	✖	✔
Xylulose 5-P → Ribose 5-P	✖	✖	✔	✔	✖	✖	✖	✔	✖	✖	✔
Ribose 5-P → Xylulose 5-P	✖	✖	✔	✔	✖	✖	✖	✔	✖	✖	✔
Xylulose 5-P + Ribose 5-P → Sedoheptulose 7-P + Glyceraldehyde 3-P	✖	✖	✔	✔	✖	✖	✖	✔	✖	✖	✔
Sedoheptulose 7-P + Glyceraldehyde 3-P → Erythrose 4-P + Fructose 6-P	✖	✖	✔	✔	✖	✖	✖	✔	✖	✖	✔
Erythrose 4-P + Xylulose 5-P → Fructose 6-P + Glyceraldehyde 3-P	✖	✖	✔	✔	✖	✖	✖	✔	✖	✖	✔
Acetate + Acetoacetyl-CoA→ Acetone + Acetyl-CoA + CO_2	✖	✖	✖	✔	✖	✖	✔	✔	✔	✖	✖
Butyrate + Acetoacetyl-CoA→ Acetone + Butyryl-CoA + CO_2	✖	✖	✖	✔	✖	✖	✔	✔	✔	✖	✖
Glucose→Pyruvate	✔	✖	✖	✖	✖	✖	✔	✖	✖	✖	✖
Butyryl -CoA → Cells	✖	✖	✖	✖	✖	✖	✔	✖	✖	✖	✔
Cells → Inactive Cells	✖	✖	✖	✖	✖	✖	✔	✖	✖	✖	✔
Xylose →Pyruvate	✖	✖	✖	✖	✖	✖	✔	✖	✖	✖	✖
Cells → Inactive Cells	✖	✖	✖	✖	✖	✖	✔	✖	✖	✖	✖
Glucose → Cells	✖	✖	✖	✖	✔	✖	✖	✖	✖	✖	✖
Butyryl-CoA + Acetate → Acetyl-CoA + Butyrate	✔	✖	✖	✖	✖	✖	✖	✖	✖	✖	✖
Acetyl-CoA + Butyrate →Butyryl-CoA + Acetate	✔	✖	✖	✖	✖	✖	✖	✖	✖	✖	✖
Acetoacetyl-CoA→ β-OH-Butyryl-CoA	✔	✖	✖	✖	✖	✖	✖	✖	✖	✖	✖
β-OH-Butyryl-CoA → Cronotyl-CoA	✔	✖	✖	✖	✖	✖	✖	✖	✖	✖	✖
Cronotyl-CoA →Butyryl-CoA	✔	✖	✖	✖	✖	✖	✖	✖	✖	✖	✖
NAD + → NADH	✖	✖	✖	✖	✖	✖	✖	✖	✖	✔	✖
NADH → NAD^+	✖	✖	✖	✖	✖	✖	✖	✖	✖	✔	✖
NADP + → NADPH	✖	✖	✖	✖	✖	✖	✖	✖	✖	✔	✖
NADPH → $NADP^+$	✖	✖	✖	✖	✖	✖	✖	✖	✖	✔	✖
NADH + FdOx → NAD^+ + FdRed	✖	✖	✖	✖	✖	✖	✖	✖	✖	✔	✖
NADP + + FdRed → NADPH + FdOx	✖	✖	✖	✖	✖	✖	✖	✖	✖	✔	✖
FdRed → FdOX + H2	✖	✖	✖	✖	✖	✖	✖	✖	✖	✔	✖
HMF → HMF Alcohol	✖	✖	✖	✖	✖	✖	✖	✖	✖	✖	✔
Furfural → Furfural Alcohol	✖	✖	✖	✖	✖	✖	✖	✖	✖	✔	✔
Total number of chemical reactions	15	19	25	27	17	19	16	23	18	27	31
Total number of chemical compounds	17	21	26	24	16	21	13	19	15	25	29
Total number of parameters	27	45	57	69	35	51	57	69	57	78	85

[a]: Votruba et al. [39].
[b]: Shinto et al. [16].
[c]: Shinto et al. [19].
[d]: Raganati et al. [22].
[e]: Buehler and Mesbah [17].
[f]: Lin and Lee [18].
[g]: Díaz and Willis [11].
[h]: Zhou et al. [20].
[i]: Zhou et al. [30].
[j]: Rivera et al. [21].

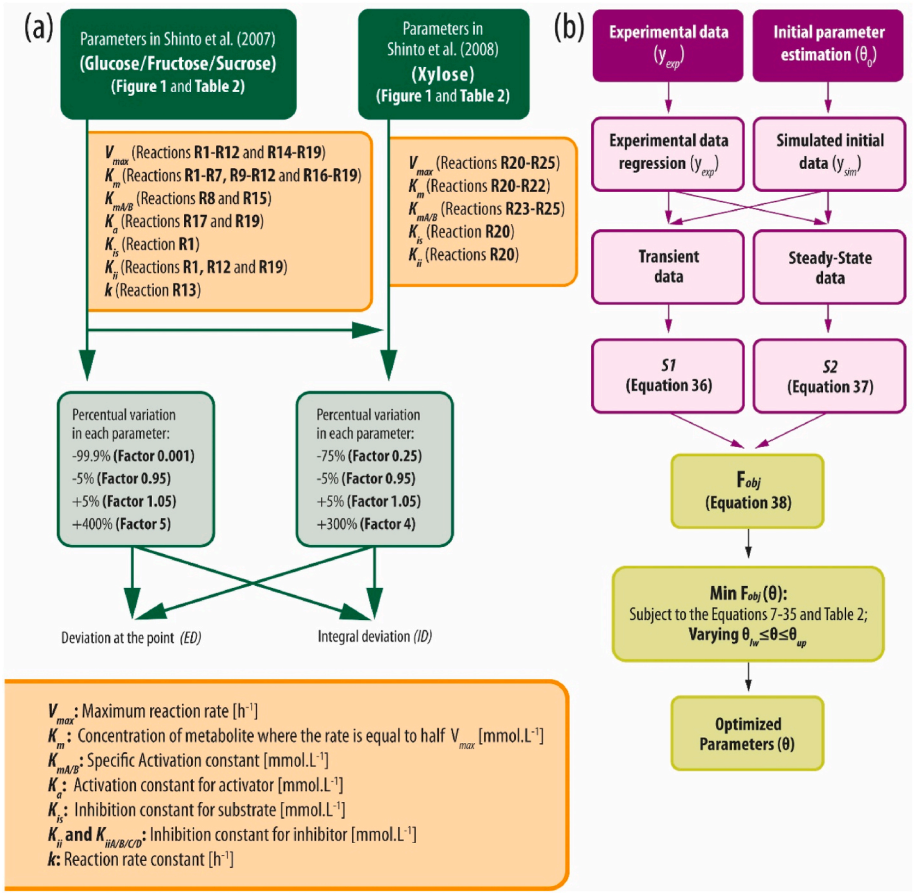

Fig. 1. **(a)** Flowchart illustrating the adopted parameter sensitivity analysis strategy. **(b)** Flowchart depicting the parameter optimization strategy implemented in *Scilab*®.

Equation (5)). This approach is schematized in Fig. 1a, and the code in *Scilab*® is available in Supplementary Material **S-2**.

$$ED\ (\%) = 100 \times \frac{[\text{Butanol}]_{end,change\ (\%)} - [\text{Butanol}]_{end,control}}{[\text{Butanol}]_{end,control}} \tag{4}$$

$$ID\ (\%) = 100 \times \sum_{t=0}^{t} \left(\frac{ABT_{t,change\ (\%)} - ABT_{t,control}}{ABT_{t,control}} \right) \tag{5}$$

Equation (6) determines the mean area of butanol concentration between time t(h) and t+1(h) (ABTt). ABTt, change (%) represents the percentage change of ABTt caused by the factors.

$$ABT_t = \frac{[\text{Butanol}]_t + [\text{Butanol}]_{t+1}}{2} \times \Delta t \tag{6}$$

where $[\text{Butanol}]_t$ indicates the butanol concentration at time t and $[\text{Butanol}]_{t+1}$ indicates the butanol concentration at time $t+1$, Δt is the difference in time but can be considered equal to 1h since this term cancels out, and $[\text{Butanol}]_{end,change(\%)}$ is the percentage change in butanol concentration at the end of the process. The results of the sensitivity analyses were used to define the kinetic model in this study.

2.3. Co-fermentation modeling framework

A structured mathematical model of the ABE fermentation of sugars and furaldehydes co-utilization by *C. saccharoperbutilacetonicum N1-4* following the metabolic route (Fig. 2) was developed to describe the rates of consumption of the carbon sources (glucose, fructose, sucrose, xylose, and arabinose), rates of formation of the products, rates of consumption and formation of the intermediate compounds, and the rates of growth and cell death, based on the models developed by Shinto et al. [16] and Shinto et al. [19] as well as the models of Díaz and Willis [11] and Rivera et al. [21].

Table 2 shows the kinetic rates of reactions in the metabolic pathway, as shown in Fig. 2. The metabolic pathway shown in Fig. 2 was used to model three distinct carbon sources. Under M75HH25, all metabolic reactions were active. On the other hand, in M100, the concentrations of pentoses, furfural, and HMF sugars were all zero, resulting in deactivation of pentose phosphate (PP) metabolism reactions (R20-R25 and R29 reactions), as well as the R32 and R33 reactions, which do not influence metabolism. In M75CHH25, the furfural concentration was zero, deactivating the R32 reaction (Supplementary Material **S-3**). The hypotheses assumed in this study are as follows:

- The volume, temperature, and pH of the reaction medium were assumed constant, and fermentation was performed using a batch system.
- Three inhibition/activation proposals were evaluated: noncompetitive inhibition by butanol (Model I), as in the model of Shinto et al. [16]; non-competitive inhibition/activation achieved using butanol, furfural, and HMF (Model II); and non-competitive inhibition/activation achieved using butanol, furfural, HMF, butyric acid, and acetic acid (Model III). Unlike the models proposed by Shinto et al. [16] and Shinto et al. [19], butyryl-CoA, but not acetyl-CoA, is the limiting compound for cell growth.
- The rate of cell death followed a first-order kinetics for cell concentration.
- The consumption rates of the carbon sources are activated and inhibited by their concentrations and undergo non-competitive inhibition by butanol.

Table 2
Kinetic rates for the dynamic ABE fermentation model.

Reaction	Model-development-kinetics equations	Ref.
Glucose → Fructose 6-P (F6P)	$R1 = \frac{V_{max\,1}[\text{Glucose}][\text{Cells}]}{\left\{K_{m1}\left(1+\frac{[\text{Glucose}]}{K_{is1}}\right)+[\text{Glucose}]\left(1+\frac{[\text{Butanol}]}{Kii_1}\right)\right\}} \times F$	[b]
Fructose 6-P → Glyceraldehyde 3-P (G3P)	$R2 = \frac{V_{max\,2}[\text{F6P}][\text{Cells}]}{K_{m2}+[\text{F6P}]} \times F$	[b]
Glyceraldehyde 3-P → Pyruvate (Pyr)	$R3 = \frac{V_{max\,3}[\text{G3P}][\text{Cells}]}{K_{m3}+[\text{G3P}]} \times F$	[b]
Lactate → Pyruvate	$R4 = \frac{V_{max\,4}[\text{Lactate}][\text{Cells}]}{K_{m4}+[\text{Lactate}]} \times F$	[b]
Pyruvate → Lactate	$R5 = \frac{V_{max\,5}[\text{Pyr}][\text{Cells}]}{K_{m5}+[\text{Pyr}]} \times F$	[b]
Pyruvate → Acetyl-CoA (ACoA) + 2 CO_2	$R6 = \frac{V_{max\,6}[\text{Pyr}][\text{Cells}]}{K_{m6}+[\text{Pyr}]} \times F$	[b]
Acetic Acid → Acetyl-P→Acetyl-CoA	$R7 = \frac{V_{max\,7}[\text{Acetic Acid}][\text{Cells}]}{K_{m7}+[\text{Acetic Acid}]} \times F$	[b]
Acetic Acid + Acetoacetyl-CoA (AACoA) →Acetoacetate + Acetyl-CoA	$R8 = [V_{max\,8}] \times \left(\frac{1}{1+K_{m8A}/[\text{Acetic Acid}]}\right) \times \left(\frac{1}{1+K_{m8B}/[\text{AACoA}]}\right) \times [\text{Cells}]$	[b]
Acetyl-CoA → Acetyl-P → Acetic Acid	$R9 = \frac{V_{max\,9}[\text{ACoA}][\text{Cells}]}{K_{m9}+[\text{ACoA}]} \times F$	[b]
Acetyl-CoA → Acetoacetyl-CoA + CoA	$R10 = \frac{V_{max\,10}[\text{ACoA}][\text{Cells}]}{K_{m10}+[\text{ACoA}]}$	[b]
Acetyl-CoA → Acetaldehyde → Ethanol	$R11 = \frac{V_{max\,11}[\text{ACoA}][\text{Cells}]}{K_{m11}+[\text{ACoA}]} \times F$	[b]
Acetoacetyl-CoA → Butyryl-CoA (BCoA)	$R14 = \frac{V_{max\,14}[\text{AACoA}][\text{Cells}]}{K_{m14}+[\text{AACoA}]} \times F$	[b]
Butyric Acid + Acetoacetyl-CoA →Acetoacetate + Butyryl-CoA	$R15 = [V_{max\,15}] \times \left(\frac{1}{1+K_{m15A}/[\text{Butyric Acid}]}\right) \times \left(\frac{1}{1+K_{m15B}/[\text{AACoA}]}\right) \times [\text{Cells}]$	[b]
Acetoacetate → Acetone + CO_2	$R16 = \frac{V_{max\,16}[\text{Acetoacetate}][\text{Cells}]}{K_{m16}+[\text{Acetoacetate}]}$	[b]
Butyric Acid → Butyryl-P → Butyryl-CoA	$R17 = \frac{V_{max\,17}[\text{Butyric Acid}][\text{Cells}]}{K_{m17}\left(1+\frac{K_{a17}}{[\text{Butyric Acid}]}\right)+[\text{Butyric Acid}]} \times F$	[b]
Butyryl-CoA → Butyryl-P → Butyric Acid	$R18 = \frac{V_{max\,18}[\text{BCoA}][\text{Cells}]}{K_{m18}+[\text{BCoA}]} \times F$	[b]
Butyryl-CoA → Butyraldehyde → Butanol	$R19 = \frac{V_{max\,19}[\text{BCoA}][\text{Cells}]}{\left\{K_{m19}\left(1+\frac{K_{a19}}{[\text{Butyric Acid}]}\right)+[\text{BCoA}]\left(1+\frac{[\text{Butanol}]}{K_{ii19}}\right)\right\}} \times F$	[b]
Xylose → Xylulose 5-P (X5P)	$R20 = \frac{V_{max\,20}[\text{Xylose}][\text{Cells}]}{\left\{K_{m20}\left(1+\frac{[\text{Xylose}]}{K_{is20}}\right)+[\text{Xylose}]\left(1+\frac{[\text{Butanol}]}{Kii_{20}}\right)\right\}} \times F$	[c]
Xylulose 5-P → Ribose 5-P (R5P)	$R21 = \frac{V_{max\,21}[\text{X5P}][\text{Cells}]}{K_{m21}+[\text{X5P}]}$	[c]
Ribose 5-P → Xylulose 5-P	$R22 = \frac{V_{max\,22}[\text{R5P}][\text{Cells}]}{K_{m22}+[\text{R5P}]}$	[c]
Xylulose 5-P + Ribose 5-P →Sedoheptulose 7-P (S7P) + Glyceraldehyde 3-P	$R23 = [V_{max\,23}] \times \left(\frac{1}{1+K_{m23A}/[\text{R5P}]}\right) \times \left(\frac{1}{1+K_{m23B}/[\text{X5P}]}\right) \times [\text{Cells}]$	[c]
Sedoheptulose 7-P + Glyceraldehyde 3-P→ Erythrose 4-P (E4P) + Fructose 6-P	$R24 = [V_{max\,24}] \times \left(\frac{1}{1+K_{m24A}/[\text{S7P}]}\right) \times \left(\frac{1}{1+K_{m24B}/[\text{G3P}]}\right) \times [\text{Cells}]$	[c]
Erythrose 4-P + Xylulose 5-P → Fructose 6-P + Glyceraldehyde 3-P	$R25 = [V_{max\,25}] \times \left(\frac{1}{1+K_{m25A}/[\text{X5P}]}\right) \times \left(\frac{1}{1+K_{m25B}/[\text{E4P}]}\right) \times [\text{Cells}]$	[c]
Sucrose → Sucrose 6-P	$R26 = \frac{V_{max\,26}[\text{Sucrose}][\text{Cells}]}{\left\{K_{m26}\left(1+\frac{[\text{Sucrose}]}{K_{is26}}\right)+[\text{Sucrose}]\left(1+\frac{[\text{Butanol}]}{Kii_{26}}\right)\right\}} \times F$	This work
Sucrose 6-P → Fructose 6-P	$R27 = \frac{V_{max\,27}[\text{Sucrose 6}-\text{P}][\text{Cells}]}{K_{m27}+[\text{Sucrose 6}-\text{P}]}$	This work
Fructose → Fructose 6-P	$R28 = \frac{V_{max\,28}[\text{Fructose}][\text{Cells}]}{\left\{K_{m28}\left(1+\frac{[\text{Fructose}]}{K_{is28}}\right)+[\text{Fructose}]\left(1+\frac{[\text{Butanol}]}{Kii_{28}}\right)\right\}} \times F$	This work
Arabinose → Ribose 5-P	$R29 = \frac{V_{max\,29}[\text{Arabinose}][\text{Cells}]}{\left\{K_{m29}\left(1+\frac{[\text{Arabinose}]}{K_{is29}}\right)+[\text{Arabinose}]\left(1+\frac{[\text{Butanol}]}{Kii_{29}}\right)\right\}} \times F$	This work
Butyryl-CoA → Cells Model I	$R30 = \frac{V_{max\,30}[\text{BCoA}][\text{Cells}]}{\{K_{m30}(1+[\text{Butanol}]/K_{ii30})+[\text{BCoA}](1+[\text{Butanol}]/Kii_{30})\}}$	[b]
Butyryl-CoA → Cells Model II	$R30 = \frac{V_{max\,30}[BCoA][Cells]}{\{K_{m30}(1+[\text{Butanol}]/K_{ii30})+[BCoA](1+[\text{Butanol}]/Kii_{30}+[\text{Furfural}]/K_{ii30A}+[\text{HMF}]/K_{ii30B})\}}$	This work

(*continued on next page*)

Table 2 (*continued*)

Reaction	Model-development-kinetics equations	Ref.
Butyryl-CoA → Cells Model III	$R30 = \frac{V_{max\ 30}[BCoA][Cells]}{\{K_{m30}(1+[Butanol]/K_{ii30})+[BCoA](1+[Butanol]/Kii_{30}+[Furfural]/K_{ii30A}+[HMF]/K_{ii30B}+[Butyric\ Acid]/K_{ii30C}+[Acetic\ Acid]/K_{ii30D})\}}$	This work
Cells → Inactives Cells	$R31 = k_{31}[Cells]$	[b]
Furfural → Furfural Alcohol	$R32 = \frac{V_{max\ 32}[Furfural][Cells]}{K_{m32}+[Furfural]} \times F$	[j]
HMF → HMF Alcohol	$R33 = \frac{V_{max\ 33}[HMF][Cells]}{K_{m33}+[HMF]} \times F$	This work
Factor F	$F = 0.5 \times (1.0 + \tanh(500 \times ([glucose]+[Fructose]+[Sucrose]+[Xylose]+[Arabinose]\text{-}1.0)))$	This work
Fator ω	$\omega = \left(\frac{[glucose]+[Fructose]+[Sucrose]}{[glucose]+[Fructose]+[Sucrose]+[Xylose]+[Arabinose]}\right)^{n_{c6/c5}}$	This work

[b]: Shinto et al. [16].
[c]: Shinto et al. [19].
[j]: Rivera et al. [21].

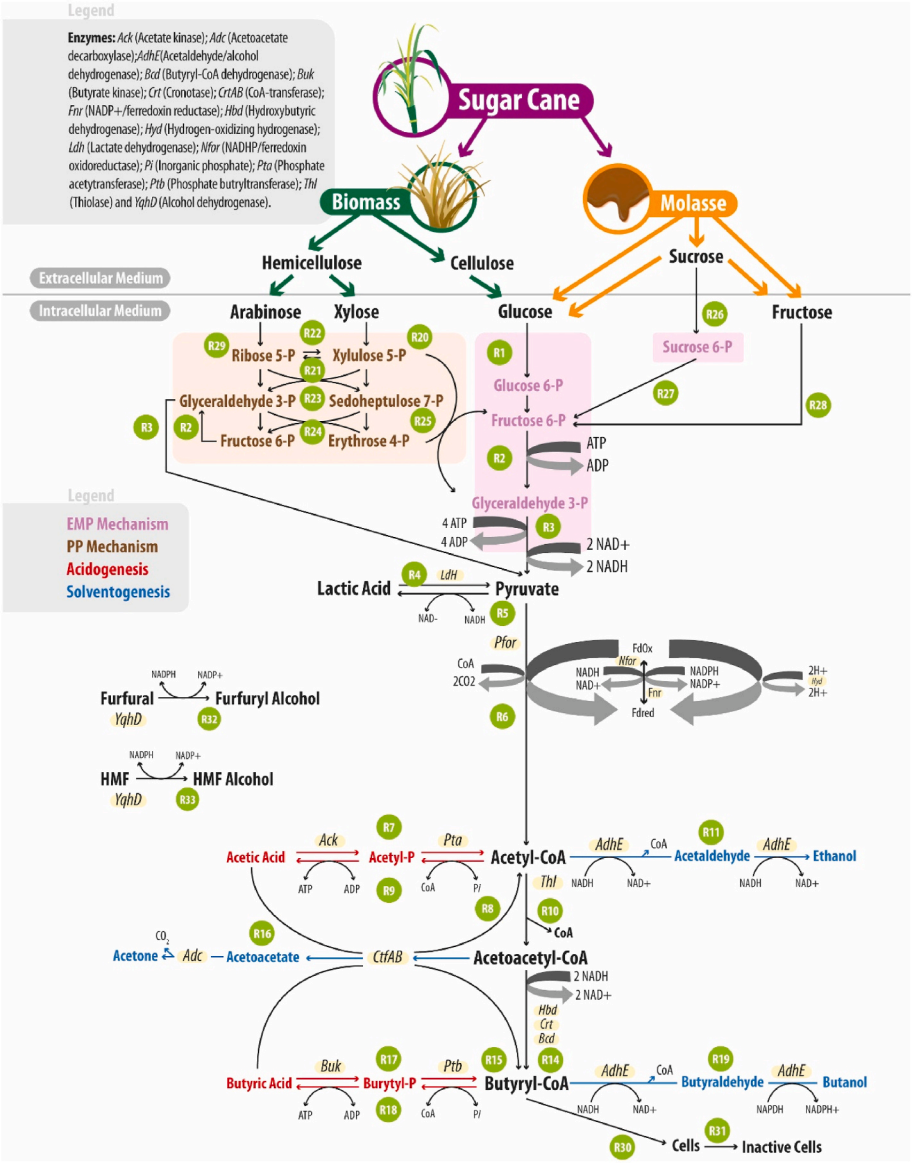

Fig. 2. Metabolic pathways for co-utilization of mixed carbon sources and furaldehydes from sugarcane biorefinery residues.

- Reactions with multiple carbon sources (R8, R15, R23, R24, and R25; Fig. 2) follow the "ping-pong" mechanism.
- The butyric acid concentration activates the conversion of butyric acid to butyryl-CoA.
- Energy is required for these reactions to occur. ATP and NADH supply this energy. When the sugar concentration falls below a critical level and microbial metabolism is no longer capable of generating energy, reactions are halted. To illustrate this phenomenon, Shinto et al. [16] and Shinto et al. [19] introduced an "on-off" mechanism (Factor *F*). This mechanism assumes a value of 1 when the carbon source concentration is greater than 1 mmol L^{-1} (critical value) and 0 when the carbon source concentration is below the critical value.
- In this study, the *F* factor (Table 2) was modified based on the hyperbolic tangent to represent smoother energy depletion. The value of *F* ranged from 1 to 0 as the total carbon source concentration decreased during fermentation: it is greater than 0.99995 and less than 0.00005 for carbon source concentrations equal or greater than 1.01 mmol L^{-1} and equal or less than 0.99 mmol L^{-1}, respectively.
- Hexoses and sucrose are consumed according to the "Embden-Meyerhof-Parnas" (EMP) metabolism, and pentoses, such as xylose and arabinose, with the "pentose phosphate" (PP) metabolism. However, in contrast to the models proposed by Shinto et al. [16] and Shinto et al. [19], in which routes are evaluated individually, our model considers all the routes simultaneously.
- Mathematical modeling of the greater preference of hexose sugars for pentose sugars (preferential use of hexoses over pentose or PUHEPE) was based on factor ω, first introduced by Díaz and Willis [11] and modified in this study. The exponent $n_{c6/c5}$ in ω is a parameter to be optimized (Table 2). The value of the optimized exponent indicates the intensity of PUHEPE. A value tending to 1 implies a weak PUHEPE, whereas a value tending to zero indicates a strong preference for hexoses [11].
- This study modified the factor ω (Table 2) to include sugars other than glucose and xylose. Thus, the glucose concentration was replaced by the total concentration of hexoses (glucose, fructose, and the disaccharide sucrose or *C6*) and the xylose concentration was replaced by the concentration of pentose sugars (xylose and arabinose or *C5*).
- The reduction reaction rate of furfural to furfuryl alcohol was modeled using Michaelis-Menten kinetics, according to the model of Rivera et al. [21]. This study adopted the same premise concerning HMF production rate in the 2,5-bis(hydroxymethyl)furan reaction (HMF alcohol).

Equations (7)–(35) represent the mass balance of the batch system and the reaction rates of chemical species at constant volume in the metabolic pathway described in Fig. 2.

$$\frac{d[Glucose]}{dt} = -R1 \times \omega \quad (7)$$

$$\frac{d[Fructose]}{dt} = -R28 \times \omega \quad (8)$$

$$\frac{d[Sucrose]}{dt} = -R26 \times \omega \quad (9)$$

$$\frac{d[Sucrose\ 6-P]}{dt} = (R26 \times \omega) - R27 \quad (10)$$

$$\frac{d[Fructose\ 6-P]}{dt} = (R1 \times \omega) + R24 + R25 + R27 + (R28 \times \omega) - R2 \quad (11)$$

$$\frac{d[Glyceraldehyde\ 3-P]}{dt} = R2 + R23 + R25 - R3 - R24 \quad (12)$$

$$\frac{d[Pyruvate]}{dt} = R3 + R4 - R5 - R6 \quad (13)$$

$$\frac{d[Lactate]}{dt} = R5 - R4 \quad (14)$$

$$\frac{d[Acetyl-CoA]}{dt} = R6 + R7 + R8 - R9 - R10 - R11 \quad (15)$$

$$\frac{d[Cells]}{dt} = R30 - R31 \quad (16)$$

$$\frac{d[Acetic\ Acid]}{dt} = R9 - R7 - R8 \quad (17)$$

$$\frac{d[Etanol]}{dt} = R11 \quad (18)$$

$$\frac{d[Acetoacetyl-CoA]}{dt} = R10 - R8 - R14 - R15 \quad (19)$$

$$\frac{d[Acetoacetate]}{dt} = R8 + R15 - R16 \quad (20)$$

$$\frac{d[Butyryl-CoA]}{dt} = R14 + R15 + R17 - R18 - R19 - R30 \quad (21)$$

$$\frac{d[Butyric\ Acid]}{dt} = R18 - R15 - R17 \quad (22)$$

$$\frac{d[CO_2]}{dt} = 2R6 + R16 \quad (23)$$

$$\frac{d[Acetone]}{dt} = R16 \quad (24)$$

$$\frac{d[Butanol]}{dt} = R19 \quad (25)$$

$$\frac{d[Xylose]}{dt} = -R20 \times (1-\omega) \quad (26)$$

$$\frac{d[Arabinose]}{dt} = -R29 \times (1-\omega) \quad (27)$$

$$\frac{d[Xylulose\ 5-P]}{dt} = R20 \times (1-\omega) + R22 - R21 - R23 - R25 \quad (28)$$

$$\frac{d[Ribose\ 5-P]}{dt} = R21 + R29 \times (1-\omega) - R22 - R23 \quad (29)$$

$$\frac{d[Sedoheptulose\ 7-P]}{dt} = R23 - R24 \quad (30)$$

$$\frac{d[Erythrose\ 4-P]}{dt} = R24 - R25 \quad (31)$$

$$\frac{d[Furfural]}{dt} = -R32 \quad (32)$$

$$\frac{d[Furfural\ alcohol]}{dt} = +R32 \quad (33)$$

$$\frac{d[HMF]}{dt} = -R33 \quad (34)$$

$$\frac{d[HMF\ alcohol]}{dt} = +R33 \quad (35)$$

Computer modeling and simulations were performed using *Scilab*® 2023.1.0 software on an Intel(R) Core(TM) i7-2600 CPU @ 3.40 GHz. To solve the system of ordinary differential equations described by

Equations (7)–(35), the "*ODE*" function was used, with the "*Stiff*" option selected, which is more appropriate for rigid systems.

2.4. Estimation of kinetic parameters

The kinetic rate equations include 85 parameters (Table 2). The optimization routine employed the *Ipopt* function available in the *Atoms tool package* (usage code developed in this study and available in Supplementary Material **S-4**). According to the strategy outlined in Fig. 1b, the parameters were optimized using the experimental data for the M75HH25 and M75CHH25 conditions reported in this study and [6], respectively. To increase the amount of available data, the experimental data for these conditions underwent nonlinear regression using *TableCurve 2D® v5.01* software. The sets of optimized parameters (θ) for M75HH25 and M75CHH25 were used to simulate pure molasses (M100). The simulation of molasses using the parameters of condition M75HH25 was referred to as M100-1, whereas that using the parameters of condition M75CHH25 was referred to as M100-2.

2.4.1. Kinetic parameter optimization strategy

The objective function (F_{obj}) to be minimized by the *Ipopt solver* consisted of the squared difference in the concentration (mmol.L^{-1}) of the experimental data ($y_{\exp}$) and the values predicted by the model (y_{sim}) divided by the arithmetic mean of the experimental data ($y_{\exp\_mean}$) for each of the 13 compounds (N_{comp}) that were measured during the fermentation course (glucose, fructose, sucrose, cells, acetic acid, ethanol, butyric acid, acetone, butanol, xylose, arabinose, furfural, and HMF). Owing to the high uncertainty of the experimental values during the stationary stage of the process, the objective function is divided into two summation terms. The first summation (s_1) stores the quadratic difference during the transient step of fermentation and the second summation (s_2) stores the difference in the stationary step of the fermentation process. The summation s_1 calculates the squared difference between the experimental and simulated data, starting from the first dataset point and ending at the last data point in the transient regime (*jci*: cutoff point of the transient state for the *j*-th compound) (**Equation (36)**). It is important to note that the *jci* values vary for each compound. The summation s_2 starts one-time unit above the position *jci* (*jci*+1) and extends to the last point of the experimental set ($N_{\exp}$) (**Equation (37)**).

$$s_{1,j} = \frac{\sum_{i=1}^{jci}\left(\frac{y_{sim,j}(t_i;\theta) - y_{exp,j}(i)}{y_{\exp\ (j)\_mean}}\right)^2}{jci_j} \tag{36}$$

$$s_{2,j} = \frac{\sum_{i=jci+1}^{N_{exp}}\left(\frac{y_{sim,j}(t_i;\theta) - y_{exp,j}(i)}{y_{\exp\ (j)\_mean}}\right)^2}{\left(N_{exp} - jci_j\right)} \tag{37}$$

The expression for the objective function is given by **Equation (38)**.

$$F_{obj} = \sum_{j=1}^{N_{comp}} \left[pri,j \times s_{1,j} + (1 - pri,j) \times s_{2,j}\right] \times pCi(j) \tag{38}$$

Where *pri,j* indicates the weight for the data in the transient part and is equal to 0.8 for all compounds, and *pCi(j)* indicates the weight for each compound (Supplementary Material **S-3**).

2.5. Sensitivity, robustness, and identifiability

A parametric sensitivity analysis of the proposed model was conducted to highlight the critical parameters that affect ABE production through sugar and furaldehydes co-utilization, and to analyze the butanol yield. The sensitivity analysis followed the methodology detailed in **Section 2.2**. The parameters analyzed in the model were the maximum velocity rates for the reactions R1-R11 and R14-R33 ($V_{\max}$); the concentrations of the metabolites when the velocity rate is equal to half of $V_{\max}$ for the reactions R1-R7, R9-R11, R14, R16-R22 and R26-R33 (K_m); the specific activation constants for the reactions R8, R15 and R23-R25 (K_{mA} and K_{mB}); the carbon source inhibition constants for the reactions R1, R20, R26, R28 and R29 (K_{is}); The inhibition constants by butanol in the reactions R1, R19, R20, R26, R28, R29 and R30 (K_{ii}); the butyric acid activation constants for the R17 and R19 (K_a) reactions; the inhibition constants by furfural (K_{iiA}), HMF (K_{iiB}), butyric acid (K_{iiC}) and acetic acid (K_{iiD}) in the R30 reaction; the cell deactivation constant in the R31 reaction (k) and finally the exponent of the factor "ω" ($n_{c6/c5}$).

2.6. Parameter fitting and validation

The parameters of the structured model were fitted using experimental data reported in this study (for M75HH25) and by Zetty-Arenas et al. [6] (for M100 and M75CHH25). The accuracy of the estimates of the kinetic parameters and predictions of the deterministic model were analyzed using Pearson's correlation coefficient. In addition, a probability value of $p > 0.95$ was obtained for all correlations between the simulation results and experimental data.

3. Results and discussion

3.1. Specific rates in co-fermentation

Data containing the maximum specific rates obtained for each compound are presented in Table 3, and reveals that a carbon source comprising a mixture of sugars is, in most cases associated with increased rates of carbon source consumption, product formation, and cell growth. Fermentation of a mixture of xylose and glucose results in increased butanol titers, sugar consumption rates, and cell growth compared to fermentation of individual sugars [23,25]. This was evidenced by the significantly lower consumption rates observed by Raganati et al. [22] [glucose 0.09735 g.gdw^{-1}. h^{-1}; and fructose 0.0727 g.gdw^{-1}.h^{-1}, sucrose 0.04212 g.gdw^{-1}.h^{-1}, xylose 0.08568 g.gdw^{-1}. h^{-1} and arabinose 0.06904 g.gdw^{-1}. h^{-1}], compared to the rates achieved in this study with a maximum butanol production rate of 0.34 ± 0.02 g.gdw^{-1}. h^{-1} and maximum cell growth rate of 0.17 ± 0.09 h^{-1} (Table 3). Thus, having as carbon source mixed sugars from the biorefinery such as hemicellulosic hydrolysate and sugarcane molasses, it is necessary to highlight the impact of metabolic reactions on solvent production caused by the presence of butanol-furaldehydes and butanol-furaldehyde-organic acids, not yet reported in structured models existing in the literature.

3.2. Multi-input-multi-output sensitivity of published kinetics models

Examination of the accuracy and reliability of the model concerning the measured variables for sucrose (Fig. 3a and Supplementary Materials

Table 3
– Maximum values for the specific rates in different carbon sources.

Specific rate	Carbon source		
q_s (g.gdw^{-1}.h^{-1})	M100	M75HH25	M75CHH25
Glucose	1.23 ± 0.04	3.58 ± 0.56	2.19 ± 1.05
Fructose	0.37 ± 0.06	1.75 ± 0.31	0.85 ± 0.61
Sucrose	0.73 ± 0.01	1.31 ± 0.22	0.62 ± 0.09
Xylose	–	0.61 ± 0.23	0.41 ± 0.71
Arabinose	–	0.13 ± 0.05	0.16 ± 0.04
q_P (g.gdw^{-1}.h^{-1})	**M100**	**M75HH25**	**M75CHH25**
Butanol	0.22 ± 0.01	0.34 ± 0.02	0.27 ± 0.04
Acetone	0.03 ± 0.00	0.31 ± 0.07	0.06 ± 0.00
Ethanol	0.04 ± 0.08	0.12 ± 0.00	0.23 ± 0.23
μ (h^{-1})	**M100**	**M75HH25**	**M75CHH25**
Cells	0.12 ± 0.06	0.17 ± 0.09	0.10 ± 0.02

S-5 to S-7) showed that the consumption of this carbon source (R1 reaction, sucrose → fructose 6-P) played a pivotal role in the negative fluctuations observed in the final concentration (*ED*) and yield (*ID*) of butanol. These findings suggest that a slower rate of carbon source consumption is advantageous for the process, as a moderate decrease (factor of 0.95) in the V_{max} values of the R1 reaction is associated with an increase in both the butanol concentration (*ED*) and productivity (*ID*). However, an excessive decrease (factor of 0.001) was linked to a reduction in both the butanol concentration and productivity. Additionally, the rapid consumption of the carbon source is closely related to a sudden increase in solvent concentration and cell growth, resulting in a phenomenon known as substrate inhibition.

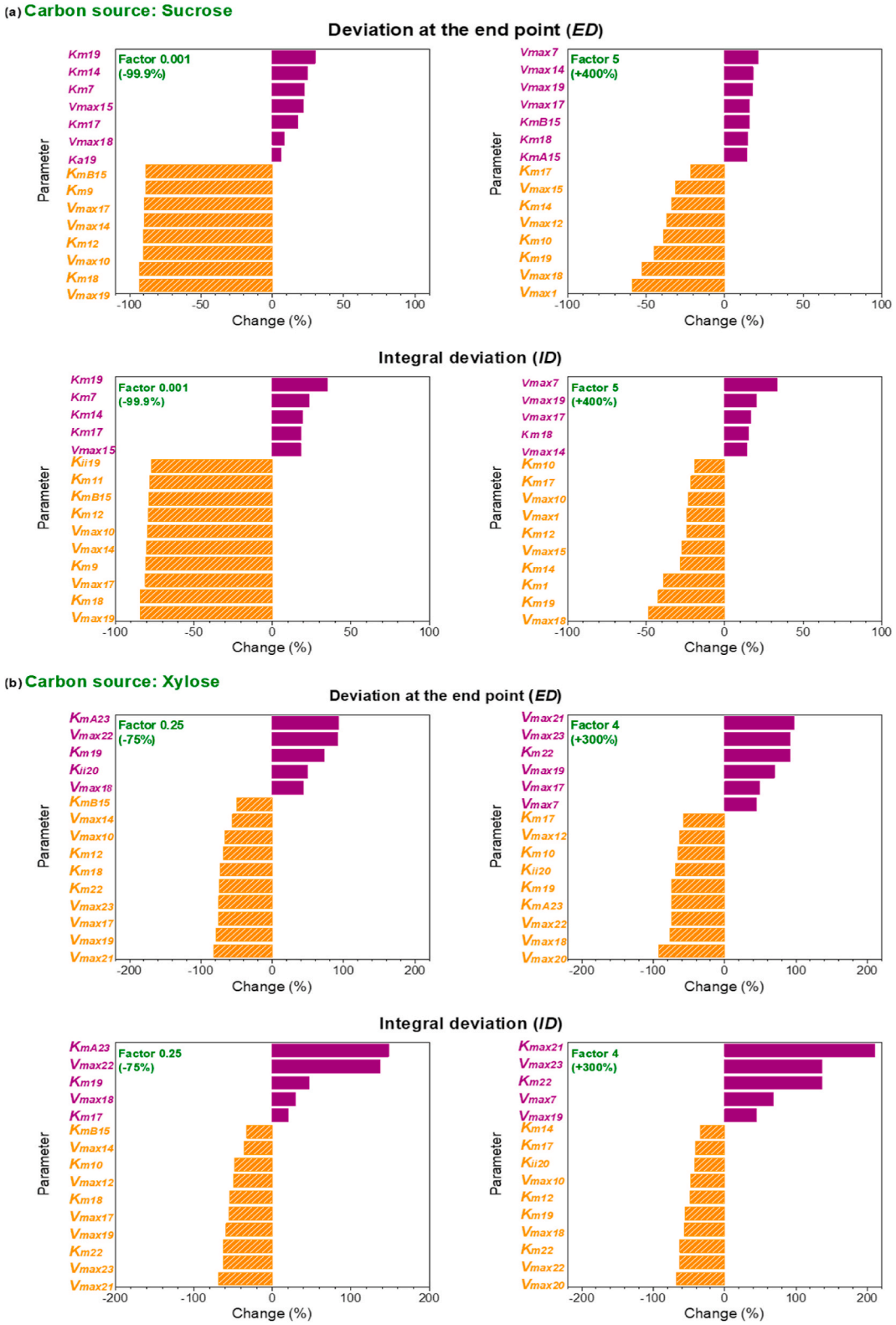

Fig. 3. Parameter sensitivity analysis of the metabolic pathways in the Shinto et al. [16] and Shinto et al. [19] models for **(a)** sucrose and **(b)** xylose.

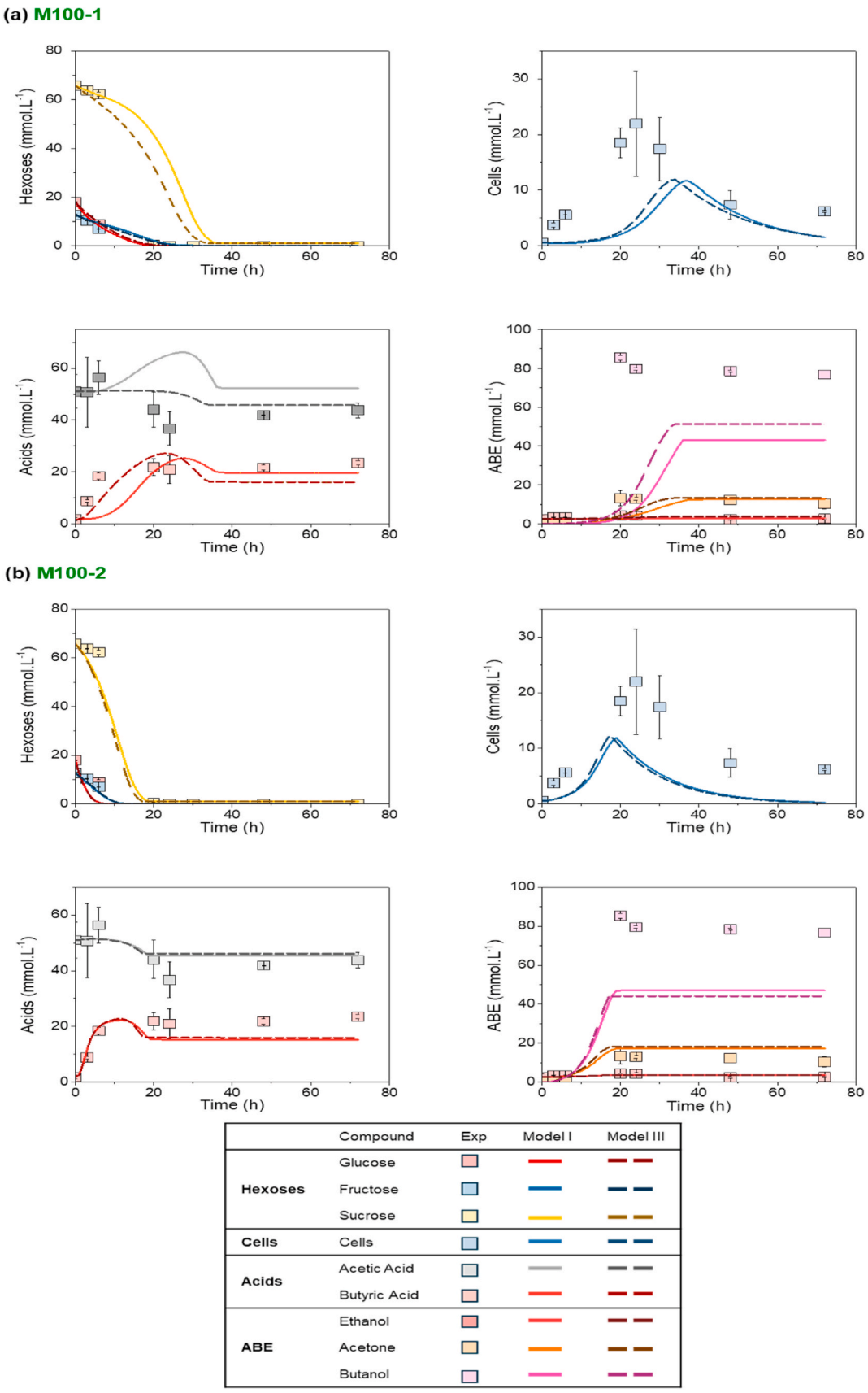

Fig. 4. Experimental time-course data and simulated results for co-utilization of carbon sources, organic acids, and ABE in **(a)** M100-1 and **(b)** M100-2 models. Experimental data (Exp) were reported by Zetty-Arenas et al. [6].

The production of butanol (R19, butyryl-CoA → butanol), which is involved in V_{max19}, positively affects the butanol yield. For the reverse reaction (R18, butyryl-CoA → butyric acid), the butanol yield is negatively affected by V_{max18}. For sucrose, the variation in V_{max19} ranged between −97.82 % and +19.47 % when analyzed by the *ED* factor and between −88.93 % and +21.73 % when analyzed by *ID* factors. The V_{max18} parameters ranged from +22.60 % to −57.06 % when analyzed by *ED* factors and from +14.17 % to −52.07 % when analyzed by *ID* factors. Similar results were obtained for fructose and glucose (Supplementary Materials **S-5** to **S-7**). Furthermore, the processes associated with the formation and consumption of CoA derivatives and the consumption of butyric acid and acetic acid are related to the increase in butanol titers, as it is believed that the pH of the fermentation medium, together with the concentration of ATP and NADH/NAD + ratio, are crucial elements that trigger the shift from the acidogenic phase to the solventogenic phase [16,29,30]. Therefore, reactions R17 (butyric acid → butyryl-CoA), R14 (acetoacetyl-CoA → butyryl-CoA), R7 (acetic acid → acetyl-CoA), and R10 (acetyl-CoA → acetoacetyl-CoA) are the main reactions associated to the increase in butanol yield.

Sensitivity analysis of xylose (Fig. 3b and Supplementary Materials **S-8**) revealed significant variations in all parameters when the factor levels were set at 0.95 and 1.05. These results suggested that the metabolic pathway for xylose consumption is highly sensitive to minor parameter variations (±5 %). The sensitivity values of all the reactions showed a strong correlation, indicating their equal importance for butanol concentration and productivity, with factors of 0.95 and 1.05. Similarly, the sensitivity analysis for xylose using factors 0.25 and 4 (Fig. 3b and Supplementary Material **S-8**) revealed, in most cases, a behavior similar to that of hexoses for most of the reactions, particularly in the shared mechanism portion (reactions R2 to R19). However, reactions R18 (butyryl-CoA to Butyric Acid) and R20 (xylose to xylulose 5-P) were the exceptions. These reactions influenced the process differently depending on the experimental conditions: low initial xylose concentration (65.7 mmol L^{-1}, reported in Supplementary Material **S-8**) and high initial xylose concentration (292 mmol L^{-1}, reported in Supplementary Material **S-8**). In the low xylose concentration condition, both R18 and R20 had negative impacts. Under conditions of high xylose concentrations (Exp. 2), R18 had a positive impact, while R20 had a positive influence with factor 0.25 and a negative influence with factor 4. In contrast, reactions R19 (butyryl-CoA → butanol), R14 (acetoacetyl-CoA → butyryl-CoA), and R7 (acetic acid → acetyl-CoA) were shown to be related to increased butanol yield.

When considering the behavior of xylose in comparison to that of hexoses, it is evident that there is a notable difference in their initial consumption mechanisms. Hexoses are metabolized through the EMP pathway and directly converted into fructose 6-P and glyceraldehyde 3-P, generating ATP and NADH. However, xylose had a distinct initiation of consumption. Initially, xylose is transformed into xylulose 5-P via the R20 reaction. Subsequently, the PP mechanism is split into two pathways to form fructose 6-P and glyceraldehyde 3-P. One pathway involves an equilibrium reaction between xylulose 5-P and ribose 5-P, which converts these compounds into sedoheptulose 7-P and glyceraldehyde 3-P, respectively, via reaction R23. The other pathway involves the reaction of xylulose 5-P with erythrose 4-P to form fructose 6-P and glyceraldehyde 3-P, respectively. Sensitivity analysis revealed that the first pathway (reactions R21, R22, and R23) had a more significant impact, with reactions R20 (except for factor 0.25 and higher initial xylose concentration) and R22 negatively influencing the final butanol concentration. Conversely, reactions R21 and R23 had a positive impact.

The implications of the findings are closely related to the subsequent discussion of the various local optima encountered by the optimization algorithm. This suggests that, while a model can be efficiently fine-tuned for practical applications, further mathematical research within the scope of this study is necessary to determine the optimal quantity of model parameters and their corresponding values.

3.3. Reaction kinetics-based modeling

The three deterministic models proposed in this study were developed through extensive optimization and simulation studies to determine the kinetic parameters of the mechanistic model.

3.3.1. Comprehensive mechanistic kinetic modeling

The optimized parameters of the model using the experimental dataset provided in this study and by Zetty-Arenas et al. [6] for the carbon sources M75HH25 and M75CHH25, respectively, are shown with two decimal places in Table 4 and with full decimal places in Supplementary Material **S-9**. The analysis of the three distinct inhibition-derived models was made possible through the results of the fitting models. Model I only considered the effect of butanol, thus capturing the stress caused solely by the solvent. Model II included the influence of furaldehydes generated during the hydrolysis of sugarcane bagasse [6], thereby considering both solvent stress and furaldehydes. Model III supplemented Model II with the influence of organic acids and provided a more comprehensive evaluation of the stress caused by the solvents, furaldehydes, and intermediate metabolites.

The parameters of the models exhibited variations, indicating that the activation or inhibition of the genetic circuit in the microorganism, which plays a crucial role in regulating metabolism and fermentation progression, can be influenced by factors such as carbohydrates, molasses, hemicellulosic hydrolysate, or a combination of these. The presence of these compounds, which are typically produced during pretreatment and biomass hydrolysis, as well as the intermediate metabolites (acetic acid and butyric acid) and final products (butanol, acetone, and ethanol), subjects the microorganism to conditions such as inappropriate pH, oxygen dissolution, osmotic pressure resulting from an uneven fermentation medium, overproduction of exogenous proteins, and enzyme suppression, which can alter cell activity and solvent titer [8,15]. ABE fermentation is highly sensitive to environmental factors, as evidenced by the significant variation in M75HH25 condition parameters among the different models. Model I had a mean relative change of 2102 % compared to Model II, whereas the variation from Model II to Model III was more moderate, with a mean relative change of 13 %. M75HH25 had a higher initial concentration of furfural (0.326 mmol L^{-1}) and HMF (0.026 mmol L^{-1}) than the other model conditions.

The parameters that exhibited the most remarkable relative variation between Models I and II were V_{max11}, V_{max18}, and V_{max15}. Similarly, the parameters that demonstrated the most remarkable relative variation between Models II and III were K_{mB8}, K_{is26}, K_{m5}, and K_{mA8}. These findings imply that the stress caused by furfural and HMF influences the production and assimilation of butyric acid and the consumption of acetyl-CoA. Butyric acid can be assimilated through various pathways, including the balance between acid and butyryl-CoA (reactions R18 and R17), the consumption of ATP and ADP, and the direct conversion of butyric acid into butyryl-CoA and acetoacetate using acetoacetyl-CoA as a CoA donor (R15 reaction). Therefore, furaldehydes can stimulate both the consumption and assimilation of butyric acid as well as the synthesis of acetone, ethanol, and butanol. The R11 reaction is related to the transformation of acetyl-CoA into ethanol, depends on the reduction of NADH/NAD+, and is mediated by acetaldehyde/alcohol hydrogenases (*AdhE*). However, these enzymes are not exclusive to ethanol synthesis, and can be used for butanol synthesis (R19 reaction) [31]. Acetic and butyric acids can stimulate the production of lactic acid (R5 reaction) and affect pH regulation in the intracellular medium, which can positively affect butanol synthesis by stimulating acetic acid consumption to form acetyl-CoA and acetoacetate (R8 reaction) and the production of lactic acid (R5 reaction). The presence of these acids is related to pH regulation in the intracellular medium. Zhou et al. [30] reported that lactic acid and acetic acid consumption positively affect butanol synthesis.

The carbon source M75CHH25 contained a purified hydrolysate with a lower concentration of furaldehydes than M75HH25. This reduces the

Table 4
Optimized parameter sets with two decimal places for the M75HH25 and M75HH25 conditions following the metabolic pathway shown in Fig. 2.

Reaction	Parameter	M75HH25			M75CHH25		
		Model I	Model II	Model III	Model I	Model II	Model III
R1	V_{max1}	74.70	464.20	410.55	441.45	438.48	446.93
R1	K_{m1}	239.68	2455.85	2122.31	653.75	655.23	648.41
R1	K_{is1}	95.80	5286.80	6052.67	6135.54	6135.43	6135.38
R1	K_{ii1}	114.20	5538.77	6471.26	7065.09	7065.05	7065.08
R2	V_{max2}	95.63	5285.69	4857.77	4786.00	4788.13	4786.64
R2	K_{m2}	133.87	944.29	987.40	645.76	631.84	640.48
R3	V_{max3}	149.76	6682.24	8551.35	12270.75	12271.86	12271.16
R3	K_{m3}	105.66	2394.73	2713.60	1841.71	1834.90	1839.94
R4	V_{max4}	130.29	758.32	749.55	747.22	747.31	747.65
R4	K_{m4}	198.26	5156.85	7419.15	8671.44	8671.77	8671.71
R5	V_{max5}	126.00	960.80	959.61	978.27	977.27	978.24
R5	K_{m5}	507.82	5174.21	7804.70	8612.24	8612.62	8612.71
R6	V_{max6}	200.85	6067.86	8013.81	10613.28	10613.73	10613.57
R6	K_{m6}	137.08	146.42	150.29	143.76	132.32	143.60
R7	V_{max7}	1.67	12.75	12.77	19.59	18.52	19.01
R7	K_{m7}	138.94	7458.59	7547.98	7521.71	7520.81	7520.95
R8	V_{max8}	78.06	2061.61	1926.25	1799.90	1800.11	1799.97
R8	K_{mA8}	112.72	2599.68	3782.49	3986.44	3986.60	3986.51
R8	K_{mB8}	127.03	2674.05	4911.48	5358.29	5358.58	5358.57
R9	V_{max9}	118.24	3496.92	3161.26	2979.44	2980.66	2980.62
R9	K_{m9}	106.64	3022.97	4038.72	3563.05	3562.31	3562.33
R10	V_{max10}	203.77	1732.26	1684.88	1917.98	1918.35	1918.63
R10	K_{m10}	138.31	116.23	109.23	98.80	99.81	89.53
R11	V_{max11}	1.74	774.35	719.34	684.12	685.33	680.74
R11	K_{m11}	191.04	3532.43	3325.15	2957.98	2958.00	2959.19
R14	V_{max14}	230.79	706.32	798.28	1181.98	1187.19	1181.24
R14	K_{m14}	99.93	637.95	599.39	363.09	345.46	365.67
R15	V_{max15}	114.51	7836.03	10495.72	11626.38	11627.26	11626.68
R15	K_{mA15}	137.80	716.52	846.88	361.23	326.26	343.89
R15	Km_{B15}	117.41	1542.50	1237.73	774.55	756.21	766.57
R16	V_{max16}	119.91	1193.40	1169.53	1191.17	1191.76	1191.45
R16	K_{m16}	122.91	988.74	976.79	995.87	995.52	995.97
R17	V_{max17}	194.68	1631.93	1895.84	3233.42	3231.55	3234.01
R17	K_{m17}	221.55	557.58	603.69	617.70	625.38	612.04
R17	K_{a17}	203.50	267.29	282.51	279.00	297.16	278.29
R18	V_{max18}	135.94	9312.72	10394.22	11090.54	11091.12	11090.44
R18	K_{m18}	105.00	644.40	617.07	669.06	655.81	668.03
R19	V_{max19}	184.18	424.29	426.37	411.52	407.17	414.97
R19	K_{m19}	92.09	50.28	61.93	49.26	40.11	48.66
R19	K_{ii19}	112.16	5059.50	6428.81	6980.71	6980.71	6980.69
R19	K_{a19}	171.41	119.30	93.84	96.22	117.27	103.50
R20	V_{max20}	59.72	99.48	106.74	107.62	138.56	122.70
R20	K_{m20}	3.16	2.58	2.36	2.48	1.35	1.00
R20	K_{is20}	11.71	12.46	12.15	13.41	12.12	11.41
R20	K_{ii20}	0.76	1.30	1.37	0.95	1.29	1.06
R21	V_{max21}	120.26	82.39	82.43	83.58	98.87	76.02
R21	K_{m21}	2.52	2.61	2.62	2.52	2.28	1.76
R22	V_{max22}	105.08	4597.42	5068.35	4921.22	4920.70	4921.72
R22	K_{m22}	2.66	2.61	2.58	2.69	3.13	2.86
R23	V_{max23}	105.87	4743.70	5153.46	5180.60	5180.52	5179.61
R23	K_{mA23}	5.09	4.94	4.57	4.80	4.52	4.26
R23	K_{mB23}	0.25	0.25	0.24	0.24	0.22	0.23
R24	V_{max24}	104.81	4668.00	5158.02	5050.22	5050.10	5049.94
R24	K_{mA24}	4.89	5.08	5.09	5.22	5.21	5.01
R24	K_{mB24}	0.25	0.25	0.24	0.25	0.26	0.26
R25	V_{max25}	113.25	5421.16	6356.75	7001.24	7001.15	7001.15
R25	K_{mA25}	5.04	4.95	4.78	5.03	4.24	4.52
R25	K_{mB25}	0.25	0.25	0.24	0.25	0.24	0.25
R26	V_{max26}	11.23	190.88	233.96	283.95	283.51	316.48
R26	K_{m26}	241.06	6149.53	6585.60	5115.89	5115.81	5113.83
R26	K_{is26}	65.44	3764.12	5887.17	5796.79	5796.88	5796.66
R26	K_{ii26}	113.26	5280.70	6466.80	6958.68	6958.67	6958.49
R27	V_{max27}	82.48	304.42	288.92	285.24	294.61	296.49
R27	K_{m27}	119.63	4573.88	5310.57	5372.82	5372.05	5372.09
R28	V_{max28}	24.42	169.16	135.48	153.75	136.97	138.89
R28	K_{m28}	200.59	1807.91	1338.42	774.68	779.05	775.56
R28	K_{is28}	102.35	4822.12	5894.69	6415.23	6414.95	6414.93
R28	K_{ii28}	113.04	5221.02	6429.09	7003.13	7003.21	7003.11
R29	V_{max29}	7.17	31.94	37.79	29.46	32.04	20.85
R29	K_{m29}	2.92	2.65	2.78	2.70	2.78	2.37
R29	K_{is29}	12.71	12.37	11.95	12.38	14.01	13.27
R29	K_{ii29}	1.93	0.93	0.83	0.79	1.33	1.60
R30	V_{max30}	20.80	63.45	70.54	73.68	82.30	76.25

(*continued on next page*)

Table 4 (*continued*)

Reaction	Parameter	M75HH25			M75CHH25		
		Model I	Model II	Model III	Model I	Model II	Model III
R30	K_{m30}	187.70	138.63	147.07	141.79	136.93	141.96
R30	K_{ii30}	131.17	2610.18	2314.56	2161.90	2161.72	2161.93
R30	K_{iiA30}		2569.11	2440.70		2162.11	2162.12
R30	K_{iiB30}		2577.47	2439.45		2162.27	2162.17
R30	K_{iiC30}			2455.49			2161.96
R30	K_{iiD30}			2430.71			2162.01
R30	$n_{C6/C5}$	0.054	0.021	0.018	0.055	0.028	0.038
R31	k_{31}	0.06	0.05	0.05	0.074	0.076	0.075
R32	V_{max32}	169.56	450.17	429.21	450.83	450.87	450.87
R32	K_{m32}	113.21	357.52	351.81	337.18	337.16	337.16
R33	V_{max33}	100.00	161.91	150.67	248.98	241.28	249.78
R33	K_{m33}	227.20	441.47	441.35	430.14	434.41	428.31

Units: V_{max} = [h^{-1}]; K_m = [mmol.L^{-1}]; K_{is} = [mmol.L^{-1}]; K_{ii} = [mmol.L^{-1}]; K_a = [mmol.L^{-1}]; $K_{mA/B}$ = [mmol.L^{-1}]; $K_{iiA/B/C/D}$ = [mmol.L^{-1}] e k_{31} = [h^{-1}].

Table 5
Pearson correlation coefficients (r^2) between the experimental and simulated data.

Compound	M100-1		M100-2		M75HH25			M75CHH25		
	a	c	a	c	a	b	c	a	b	c
Cells	0.521	0.393	0.822	0.814	0.927	0.937	0.933	0.934	0.934	0.934
Glucose	0.992	0.984	0.984	0.776	0.989	0.990	0.991	0.987	0.985	0.985
Fructuse	0.970	0.977	0.974	0.983	0.991	0.992	0.993	0.985	0.982	0.982
Sucrose	0.702	0.861	0.987	0.982	0.995	0.992	0.991	0.984	0.982	0.979
Xylose					0.951	0.962	0.961	0.975	0.968	0.961
Arabinose					0.907	0.917	0.916	0.928	0.920	0.911
Acetic Acid	0.264	0.786	0.832	0.803	0.793	0.855	0.836	0.781	0.785	0.793
Butyric Acid	0.639	0.702	0.805	0.801	0.460	0.875	0.856	0.789	0.765	0.776
Butanol	0.364	0.347	0.467	0.466	0.870	0.942	0.926	0.806	0.807	0.812
Acetone	0.474	0.841	0.986	0.986	0.850	0.919	0.911	0.984	0.986	0.987
Ethanol	0.678	0.797	0.832	0.836	0.802	0.809	0.809	0.985	0.984	0.985
Furfural					0.999	0.997	0.997			
HMF					0.928	0.942	0.941	0.330	0.327	0.33
Average	0.623	0.743	0.855	0.827	0.882	0.933	0.928	0.872	0.869	0.870

a = Model I; b = Model II; c = Model III.

influence of the carbon source characteristics. The results showed a moderate relative variation in the parameters for this condition, with a maximum mean relative variation of 5.78 % from Models I to II. The significant disparity in the optimization of parameters between the three models for the M75HH25 condition, in contrast to the uniformity of the parameters for the M75CHH25 condition, suggests the complex impact of external environmental factors. Analyzing the effects of acids, solvents, and furaldehydes using these kinetic models can provide better strategies for optimizing fermentation conditions and deepen our understanding of *Clostridium* metabolic processes.

Another essential issue in disrupting the metabolic pathway involved in butanol synthesis is the different processes involved in the carbon source transport and metabolism. Strains of the genus *Clostridium* use a combination of mechanisms known as phosphoenolpyruvate (PEP)-dependent and-non-dependent (PTSs) for glucose assimilation during ABE fermentation, with the predominance of the PTS-dependent system in the solventogenic phase. PTS systems play a fundamental role in the metabolic regulation of microorganisms and facilitate the transport of sugars such as glucose, fructose, mannose, and sucrose. In contrast, pentose sugars, such as xylose and arabinose, employ non-PTS-dependent routes for transport to the intracellular medium [8].

3.3.2. Describing sugars co-utilization

The results in Figs. 4–5, and Supplementary Material **S-10** demonstrate that combining molasses and sugarcane biorefinery hemicellulosic hydrolysate to co-utilize sugar could mitigate the effects of catabolic carbon regulation (PUHEPE) in fermentation media with moderate levels of hydrolyzed pentose sugars. However, this is insufficient in highly concentrated media, and alternative strategies, such as using strains with higher pentose sugar affinity, genetic modification, or adding more nutrients, should be explored. Table 4 indicates that the exponent $n_{c6/c5}$ of the factor ω for condition M75HH25 is 0.054, 0.021, and 0.018 for Models I, II, and III, respectively. Additionally, for M75CHH25, the optimized values of the exponent are 0.055, 0.028, and 0.038, respectively. The factor ω measures the level of competition between the distinct types of sugars in the fermentation medium. As all models exhibited $n_{c6/c5}$ values approaching zero (so ω tends to 1.0), this suggests a strong preference for microorganisms to consume hexose sugars over pentoses.

The optimized $n_{c6/c5}$ values and specific carbon source consumption rates (Table 3) suggest that the reduced use of xylose and arabinose by microorganisms does not always result in reduced butanol titers. In fact, sugars and their co-utilization may result in higher butanol titers [32], as reinforced by the specific rates (Table 3), where the M75HH25 condition presented butanol production rates higher than those of pure molasses. Minerals present within the hydrolysate medium are essential for maintaining microorganisms by regulating pH, facilitating electron transport, influencing enzyme expression, and affecting the NAD(P)H/NAD(P) + ratio [8,32]. In a study conducted by Zetty-Arenas et al. [6], it was observed that increasing the concentration of purified hydrolysate in the fermentation medium had a limiting effect in compensating for the decrease in glucose concentration in the reaction medium. Specifically, the maximum concentrations of butanol in the media composed of 50 % and 75 % hydrolysate were 4.07 g L^{-1} and 0.54 g L^{-1}, respectively, compared to 7.79 g L^{-1} for the medium with 25 % purified hydrolysate and 6.33 g L^{-1} for pure molasses.

3.3.3. Kinetic analysis of reaction progress curves

From Figs. 4–5 and Tables 5, it is possible to evaluate how the inclusion of the inhibition terms butanol (Model I), butanol and

furaldehydes (Model II), and butanol, furaldehydes, and organic acids (Model III) affects the concentration versus time profiles and Pearson's coefficient (r^2) for the 13 compounds under different experimental conditions. Significant variations in r^2 values were observed between Models I and II, particularly for cells (0.927–0.937), xylose (0.951–0.962), arabinose (0.907–0.917), butyric acid (0.460–0.875), acetic acid (0.793–0.855), butanol (0.870–0.942), and acetone (0.850–0.919), under M75HH25 conditions. The transition from Model II to Model III showed less marked variation with a slight decrease in r^2 for acetic and butyric acids. For M75CHH25, with a lower concentration of furaldehydes, slight variation was observed between the different models, which was also reflected in the M100-2 model. These results suggest that including terms for activation/inhibition by furaldehydes and organic acids had little impact on carbon source consumption, cell growth, and butanol production but affected the assimilation of organic acids in the process.

3.4. Kinetic analysis of activation and inhibition actions during sugars and furaldehydes co-utilization

The solvents generated in the ABE fermentation process, such as butanol, ethanol, and acetone, may have detrimental effects on microorganisms because of their lipophilicity, which can lead to rupture of the lipid bilayer in the cell membrane [15]. Among these solvents, butanol is the only one that can reach concentrations high enough to exert toxic effects [17]. As shown in Fig. 5, the structure of the model proposed in this study showed a maximum butanol concentration of ~70 mmol L^{-1}, which is well below the toxic limit. This suggests that the inhibitory effect of butanol in the current situation was not significant when compared to the levels reported ~176 mmol L^{-1} [14] or 108 mmol L^{-1} to 135 mmol L^{-1} [17].

Furfural and HMF are compounds formed during the hydrolysis steps of hemicellulose, and their concentrations vary between 0.8 mmol L^{-1} and 115 mmol L^{-1}, depending on the raw material and method used [33] The simulated data in this study report maximum concentrations of furfural and HMF at 0.33 mmol L^{-1} and 0.03 mmol L^{-1} (Fig. 5), respectively, and the effect on metabolism is considered stimulants for the process [33] associated with their reduction to less toxic alcohols using cofactors such as NADH and NADPH. These cofactors are also involved in butanol synthesis and NADH consumption stimulates NAD+ regeneration, thereby favoring glycolysis. However, at excessive concentrations, NADH consumption can exceed its regeneration rate, disturbing the NADH/NAD+ balance and interrupting glycolysis. The furfural and HMF concentrations obtained in this study were significantly lower than those reported previously [34].

The utilization of organic acids (Fig. 5) such as acetic acid and butyric acid to produce solvents is a complex and essential process. The pH of the intracellular environment has been proposed to play a crucial role in the production of organic acids and solvents. Cells are stimulated to produce acids at high pH levels, whereas at low pH levels, the stimulus is redirected towards the production of solvents. The addition of external acetic and butyric acids results in increased solvent productivity. However, excessively high acid concentrations can lead to acidification of the cytoplasm and the accumulation of anions, which can significantly reduce cell growth and butanol production. This phenomenon is called "acid crash" [15,35]. In this study, the maximum concentrations of acetic and butyric acids were approximately 77 mmol L^{-1} and 27 mmol L^{-1}, respectively. These concentrations were in the range considered activators for the process, similar to furfural and HMF.

All analyzed compounds had concentrations below the limits reported as toxic to microorganisms, which was reflected in the values of the inhibition findings for each of these compounds ($K_{iiA/B/C/D}$, Table 4), which ranged between 2160 and 2455 mmol L^{-1}, indicating a negligible inhibitory effect of these compounds on the process. Thus, the presence of these compounds disturbs the process, but their effects are not inhibitory but activating. The activating effect of furfural, HMF, and acids can be seen through the fact that the specific productivity rate of butanol and cell growth (Table 3) occurred under the experimental conditions M75HH25, which presented the highest concentration of these compounds. As discussed in **Section 3.5**, the sensitivity analysis of the parameters K_{a17} and K_{a19} (Figs. 6–7 and Supplementary Material **S-11**), which evaluate the affinity of the enzymes of the R17 and R19 reactions with butyric acid, indicated that an increase in the affinity of these enzymes for the acid has a positive impact on the process.

3.5. Sensitivity analysis for the kinetic model

The disturbances caused by sugars and aromatic co-utilization of multiple carbon sources motivated an in-depth analysis. This analysis also aims to compare the similarities and divergences in the impacted reaction steps with respect to the sensitivity of the literature models for individual and high-purity carbon sources.

Based on the observations derived from Figs. 6–7 using Model III and Supplementary Material **S-11**, the results show that the parameter V_{max30}, which involved in cell growth, has different impacts depending on the factors and the analysis method (*ED* or *ID*). For factors 1.05 and 5, the *ED* analysis shows that V_{max30} negatively influences the process, while the *ID* analysis shows a positive impact suggesting higher yield values for butanol concentration during most of the fermentation process. With factor 0.95, *ED* analysis shows a positive impact and *ID* analysis shows a negative impact, indicating the opposite effect compared to factors 1.05 and 5. With factor 0.001, both *ED* and *ID* analyses show a negative influence. Therefore, a strong reduction in cell growth rate (factor 0.001) has a negative effect, a slight reduction (factor 0.95) selectively favors butanol production, and an increase in cell growth rate (factors 1.05 and 5) has a positive impact on the process overall, but not selectively for butanol.

The consumption of acetic acid, acetoacetate, and butyryl-CoA to produce acetyl-CoA (R7 reaction), butyryl-CoA (R14 reaction), and butanol (R19 reaction), respectively, is directly correlated with increased productivity and the final concentration of butanol. However, butyryl-CoA consumption to produce butyric acid (R18 reaction) and cell death (R31 reaction) are associated with decreased productivity and the final concentration of butanol. The assimilation of butyric acid significantly influences the final yield of butanol, which can occur through the equilibrium between the R17 and R18 reactions and the R15 reaction. These results suggest that reducing the affinity for enzymes that promote the R18 reaction over the R17 reaction (*Buk* and *Ptb*) positively affects the process. In contrast, the R15 reaction has a negative effect, indicating that the assimilation of butyric acid by the R17 reaction is more influential. The increased affinity of the enzymes for butyric acid (K_{a17} in R17 and K_{a19} in R19) also strongly affects this process. The enhancement of enzymes that regulate the acetic acid/acetyl-CoA balance, particularly the R7 reaction (*Ack* and *Pta*) and enzymes involved in the R14 reaction (*Hbd*, *Crt*, and *Bcd*), significantly impacted the process. Furthermore, the contribution of *AdhE* was significant, as it could be utilized by the reactions responsible for producing butanol (R19 reaction) and ethanol (R11 reaction). Its performance is favorable for the R19 reaction and unfavorable for the R11 reaction.

The results in the literature are, in general, in agreement with those found in this study. Cooksley et al. [36] found that *Clostridium acetobutylicum* bacteria deficient in the *Buk* and *Ptb* enzymes and with overexpression of the *Ack* enzyme are associated with an increase in the final concentration of butanol. Similarly, Hou et al. [37] observed that the overexpression of the enzymes *Hbd, Thl*, *Crt*, and *Bcd* (reactions R10 and R14) is also related to the increase in butanol titer.

Lee et al. [38] demonstrated that the enzyme *CtfB* (in reaction R15) positively contributes to increasing butanol concentration. However, in the model proposed here, the influence of this enzyme is negative. Additionally, the positive effect of *CtfB* on butanol yield, as observed by Lee et al. [38] is less significant compared to the stronger impact of enzyme suppression in reaction R18, which shifts the balance away from

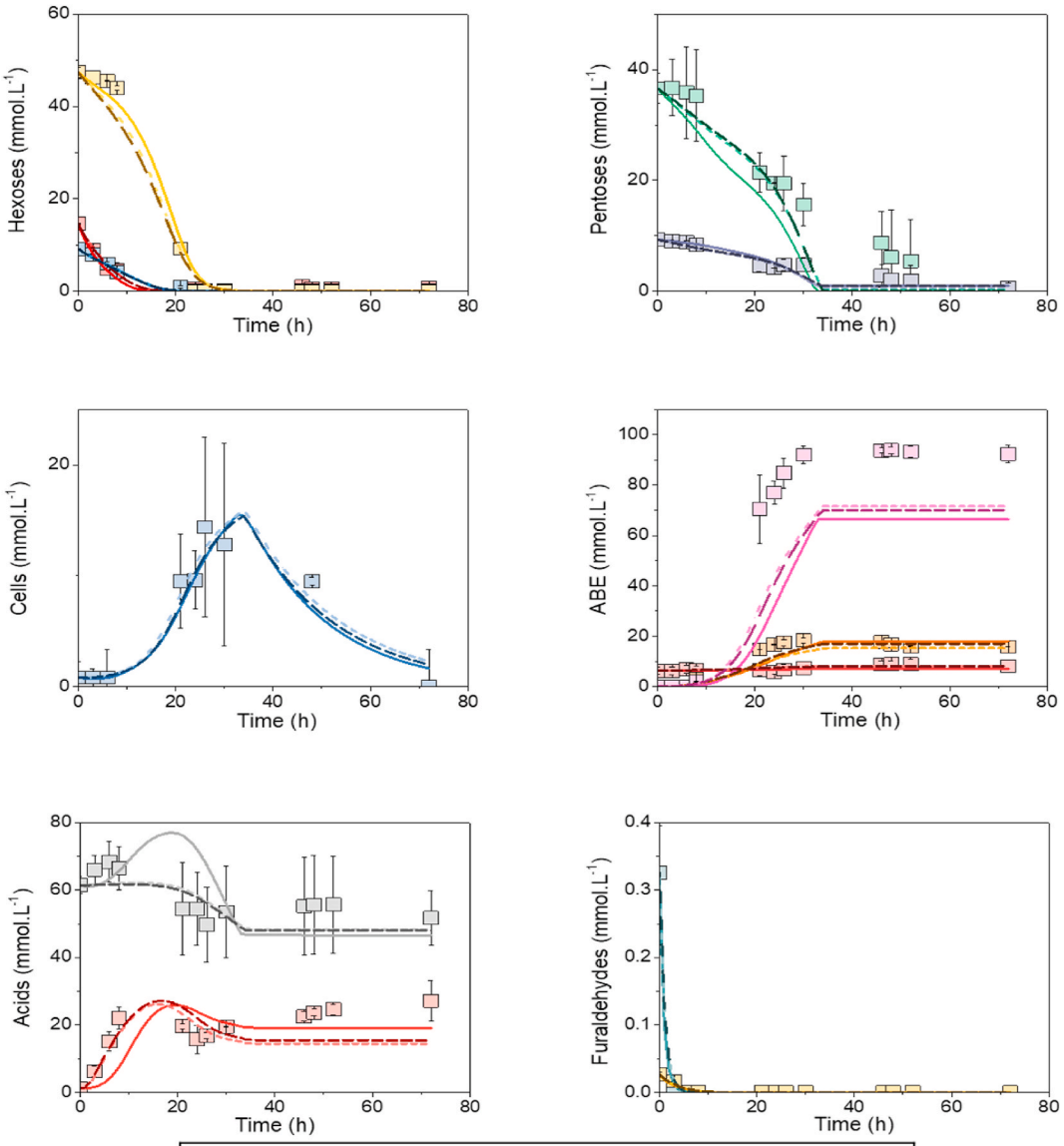

	Compound	Exp	Model I	Model II	Model III
Hexoses	Glucose				
	Fructose				
	Sucrose				
Pentoses	Xylose				
	Arabinose				
Cells	Cells				
Acids	Acetic Acid				
	Butyric Acid				
ABE	Ethanol				
	Acetone				
	Butanol				
Furaldehydes	Furfural				
	HMF				

Fig. 5. Experimental time-course data and simulated results for the co-utilization of carbon sources, organic acids, furaldehydes, and ABE in the M75HH25 model.

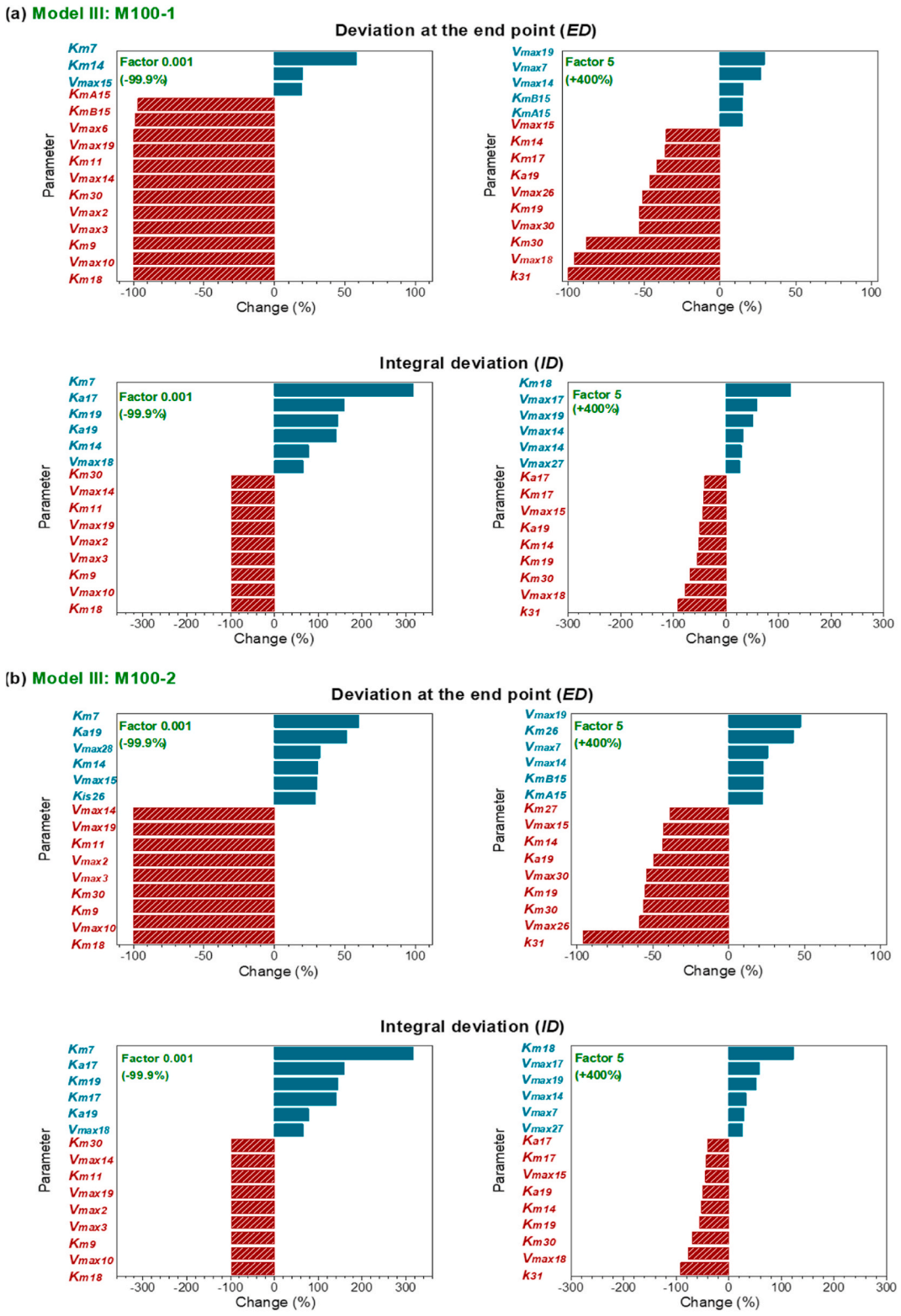

Fig. 6. Parameter sensitivity analysis for co-utilization of molasses in **(a)** M100-1 and **(b)** M100-2 models (Model III).

reaction R17 (involving *Buk* and *Ptb* enzymes), as suggested in our model.

The reactions responsible for carbon source consumption (R1, R20, R26, R28, and R29) had the most significant negative impact on the butanol yield in the analysis of individual sugars. However, when sugars and aromatics were co-utilized, these reactions had a less significant effect on the process, losing their importance in reactions R18, R9, R11, R31, and R15, which became more significant regarding the negative impacts. Additionally, the cell growth reaction (R30 reaction for multiple carbon sources or R12 reaction for a single carbon source) had a less significant effect on the analysis of the individual sugars.

The findings of the sensitivity analysis provide recommendations to optimize early-stage process design to improve the butanol production efficiency. The parameters related to reactions R7, R14, R17, and R19

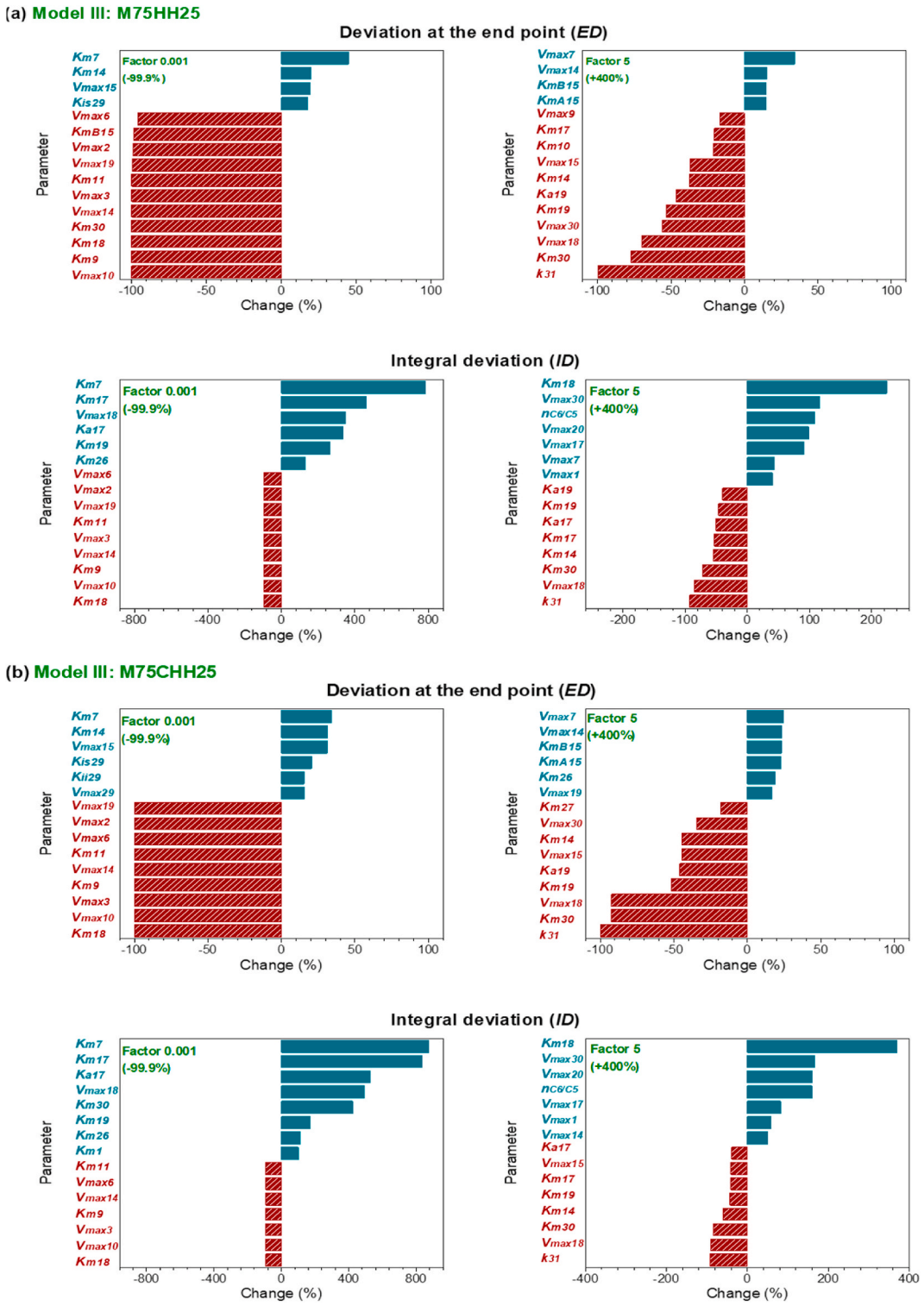

Fig. 7. Parameter sensitivity analysis for the co-fermentation of multiple carbon sources in **(a)** M75HH25 and **(b)** M75CHH25 models (Model III).

consistently demonstrated positive effects across various models, indicating their potential to enhance the butanol yield. In contrast, parameters for reactions R9, R11, R18, and R31 consistently showed adverse effects. Finally, the reactions associated with carbon source consumption and cell growth exhibited ambiguous sensitivity behavior, which was influenced by mixed/individual sugar fermentation, *ED* or *ID* analysis, and other relevant variables. Elucidating the variations in the kinetic parameters of sugar and furaldehyde co-utilization and individual sugar fermentation offers valuable insights into the obstacles faced in mixed-carbon-source environments. These findings may inform potential approaches to optimize kinetics and fine-tune metabolic pathways, thereby driving progress in butanol production.

4. Conclusion

The current study introduces three kinetic models of *C. saccharoperbutilacetonicum N1-4*'s ABE fermentation, integrating multiple carbon source fermentation and furaldehydes consumption to

highlight critical insights. The stress induced by furfural and HMF, particularly under M75HH25 conditions, influences butyric acid production, assimilation, and the synthesis of acetone, ethanol, and butanol. The involvement of multiple pathways in butyric acid assimilation highlights the complexity of the metabolic regulation. Enzyme enhancements targeting the acetic acid/acetyl-CoA balance and reactions, such as R7 (aceticacid → acetyl-CoA) and R14 (acetoacetyl-CoA→ butyryl-CoA), significantly affect the fermentation process. Furthermore, the significant contribution of *AdhE* to butanol and ethanol synthesis highlights its versatile role in various metabolic pathways. This study revealed the critical kinetic parameters influencing biobutanol production and offers valuable insights into overcoming obstacles hindering its large-scale commercialization and early-stage project design.

CRediT authorship contribution statement

Roger Assis de Oliveira: Writing – review & editing, Writing – original draft, Visualization, Validation, Methodology, Investigation, Formal analysis, Data curation, Conceptualization. **Ana Maria Zetty Arenas:** Writing – review & editing, Validation, Methodology, Investigation. **José Plácido:** Writing – review & editing, Validation, Supervision, Software, Methodology, Formal analysis. **Laura Plazas Tovar:** Writing – review & editing, Writing – original draft, Visualization, Supervision, Software, Resources, Project administration, Funding acquisition, Formal analysis, Data curation, Conceptualization.

Declaration of competing interest

The authors declare no competing financial interests or personal relationships that could influence the work reported in this study.

Acknowledgments

The authors thank the Coordenação de Aperfeiçoamento de Pessoal de Nível Superior - Brasil (CAPES) - Finance Code 001, Brazilian National Council for Scientific and Technological Development (CNPq) [grant #402900/2023–5 and #141465/2015–8], and São Paulo Research Foundation (FAPESP) [grant #2015/20630–4] for their financial support.

Appendix A. Supplementary data

Supplementary data to this article can be found online at https://doi.org/10.1016/j.biombioe.2024.107435.

Data availability

Research data supporting this publication are available from the repository at https://domusdados.unifesp.br/dataverse/ikmofabe

References

[1] A.E. García-Hernández, J.G. Segovia-Hernández, E. Sánchez-Ramírez, G. C. Zarazúa, I.F.H. Araujo, J.J. Quiroz-Ramírez, Sustainable aviation fuel from butanol: a study in optimizing Economic and Environmental impact through process intensification, Chem. Eng. Process. - Process Intensif. 200 (2024), https://doi.org/10.1016/j.cep.2024.109769.

[2] S. Prasad, K.K. Yadav, S. Kumar, P. Pandita, J.K. Bhutto, M.A. Alreshidi, B. Ravindran, Z.M. Yaseen, S.M. Osman, M.M.S. Cabral-Pinto, Review on biofuel production: sustainable development scenario, environment, and climate change perspectives – A sustainable approach, J. Environ. Chem. Eng. 12 (2024) 111996, https://doi.org/10.1016/j.jece.2024.111996.

[3] N. Amira, S. Zaidi, N.A. Jamaldin, B. Fauzi, N. Izzati, M. Ismail, Production of Butanol Using *Clostridium Acetobutylicum* in Anaerobic System, 4, 2023, pp. 91–97.

[4] M. Rivas-Astroza, I. Paredes, K. Guerrero, S. Mau, J. Quintero, J.C. Gentina, R. Conejeros, G. Aroca, Kinetic model of *Clostridium beijerinckii*'s acetone-butanol-ethanol fermentation considering metabolically diverse cell types, J. Biotechnol. 342 (2021) 1–12, https://doi.org/10.1016/j.jbiotec.2021.09.021.

[5] Y. Ni, Z. Xia, Y. Wang, Z. Sun, Continuous butanol fermentation from inexpensive sugar-based feedstocks by *Clostridium saccharobutylicum DSM 13864*, Bioresour. Technol. 129 (2013) 680–685, https://doi.org/10.1016/j.biortech.2012.11.142.

[6] A.M. Zetty-Arenas, L.P. Tovar, R.F. Alves, A.P. Mariano, W. van Gulik, R. Maciel Filho, S. Freitas, Co-fermentation of sugarcane bagasse hydrolysate and molasses by *Clostridium saccharoperbutylacetonicum*: effect on sugar consumption and butanol production, Ind. Crops Prod. 167 (2021) 113512, https://doi.org/10.1016/j.indcrop.2021.113512.

[7] C. Su, D. Cai, H. Zhang, Y. Wu, Y. Jiang, Y. Liu, C. Zhang, C. Li, P. Qin, T. Tan, Pilot-scale acetone-butanol-ethanol fermentation from corn stover, Green Carbon 2 (2024) 81–93, https://doi.org/10.1016/j.greenca.2024.02.004.

[8] Y. Guo, Y. Liu, M. Guan, H. Tang, Z. Wang, L. Lin, H. Pang, Production of butanol from lignocellulosic biomass: recent advances, challenges, and prospects, RSC Adv. 12 (2022) 18848–18863, https://doi.org/10.1039/d1ra09396g.

[9] M. Tang, J. Liu, Z. Ye, S. Zhuo, W. Zhang, X. Li, D. Chen, Exploring co-fermentation of glucose and galactose using *Clostridium acetobutylicum* and *Clostridium beijerinckii* for Biofuels, Nat. Prod. Commun. 12 (2017) 1921–1924, https://doi.org/10.1177/1934578x1701201227.

[10] A.P. Mariano, M.O.S. Dias, T.L. Junqueira, M.P. Cunha, A. Bonomi, R.M. Filho, Utilization of pentoses from sugarcane biomass: techno-economics of biogas vs. butanol production, Bioresour. Technol. 142 (2013) 390–399, https://doi.org/10.1016/j.biortech.2013.05.052.

[11] V.H.G. Díaz, M.J. Willis, Kinetic modelling and simulation of batch, continuous and cell-recycling fermentations for acetone-butanol-ethanol production using *Clostridium saccharoperbutylacetonicum N1-4*, Biochem. Eng. J. 137 (2018) 30–39, https://doi.org/10.1016/j.bej.2018.05.011.

[12] H.G. Moon, Y.S. Jang, C. Cho, J. Lee, R. Binkley, S.Y. Lee, One hundred years of clostridial butanol fermentation, FEMS Microbiol. Lett. 363 (2016), https://doi.org/10.1093/femsle/fnw001.

[13] S. Shanmugam, A. Hari, D. Kumar, K. Rajendran, T. Mathimani, A.E. Atabani, K. Brindhadevi, A. Pugazhendhi, Recent developments and strategies in genome engineering and integrated fermentation approaches for biobutanol production from microalgae, Fuel 285 (2021) 119052, https://doi.org/10.1016/j.fuel.2020.119052.

[14] N.R. Baral, A. Shah, Microbial inhibitors: formation and effects on acetone-butanol-ethanol fermentation of lignocellulosic biomass, Appl. Microbiol. Biotechnol. 98 (2014) 9151–9172, https://doi.org/10.1007/s00253-014-6106-8.

[15] S. Li, L. Huang, C. Ke, Z. Pang, L. Liu, Pathway dissection, regulation, engineering and application: lessons learned from biobutanol production by solventogenic clostridia, Biotechnol. Biofuels 13 (2020) 1–25, https://doi.org/10.1186/s13068-020-01674-3.

[16] H. Shinto, Y. Tashiro, M. Yamashita, G. Kobayashi, T. Sekiguchi, T. Hanai, Y. Kuriya, M. Okamoto, K. Sonomoto, Kinetic modeling and sensitivity analysis of acetone-butanol-ethanol production, J. Biotechnol. 131 (2007) 45–56, https://doi.org/10.1016/j.jbiotec.2007.05.005.

[17] E.A. Buehler, A. Mesbah, Kinetic study of acetone-butanol-ethanol fermentation in continuous culture, PLoS One 11 (2016) 1–21, https://doi.org/10.1371/journal.pone.0158243.

[18] T.C. Lin, Y.H. Lee, Modeling and dynamic optimization of semi-batch acetone–butanol–ethanol fermentation with in-situ pervaporation membrane separations, Smart Sci 5 (2017) 179–193, https://doi.org/10.1080/23080477.2017.1390435.

[19] H. Shinto, Y. Tashiro, G. Kobayashi, T. Sekiguchi, T. Hanai, Y. Kuriya, M. Okamoto, K. Sonomoto, Kinetic study of substrate dependency for higher butanol production in acetone-butanol-ethanol fermentation, Process Biochem. 43 (2008) 1452–1461, https://doi.org/10.1016/j.procbio.2008.06.003.

[20] Q. Zhou, H. Zheng, W. Yuan, Modeling butanol synthesis in xylose by *Clostridium saccharoperbutylacetonicum*, Bioresources 13 (2018) 7270–7280, https://doi.org/10.15376/BIORES.13.4.7270-7280.

[21] E.C. Rivera, D.C. Assumpção, H.J. Kwon, C.C. Okonkwo, T.C. Ezeji, R.M. Filho, A. P. Mariano, Mechanistic modeling of redox balance effects on the fermentation of eucalyptus wood-derived xylose to acetone-butanol-ethanol, Biochem. Eng. J. 190 (2023), https://doi.org/10.1016/j.bej.2022.108738.

[22] F. Raganati, A. Procentese, G. Olivieri, P. Götz, P. Salatino, A. Marzocchella, Kinetic study of butanol production from various sugars by *Clostridium acetobutylicum* using a dynamic model, Biochem. Eng. J. 99 (2015) 156–166, https://doi.org/10.1016/j.bej.2015.03.001.

[23] C. Birgen, O.T. Berglihn, H.A. Preisig, A. Wentzel, Kinetic study of butanol production from mixtures of glucose and xylose and investigation of different pre-growth strategies, Biochem. Eng. J. 147 (2019) 110–117, https://doi.org/10.1016/j.bej.2019.04.002.

[24] J. Lim, H.E. Byun, B. Kim, H. Park, J.H. Lee, Modeling and dynamic optimization of semi-batch acetone–butanol–ethanol fermentation with in-situ pervaporation membrane separations, Energy Fuel. 33 (2019) 8620–8631, https://doi.org/10.1021/acs.energyfuels.9b01007.

[25] J. Lim, H.E. Byun, B. Kim, J.H. Lee, Dynamic modeling of acetone-butanol-ethanol fermentation with ex situ butanol recovery using glucose/xylose mixtures, Ind. Eng. Chem. Res. 59 (2020) 2581–2592, https://doi.org/10.1021/acs.iecr.9b03016.

[26] C. Liao, S.O. Seo, V. Celik, H. Liu, W. Kong, Y. Wang, H. Blaschek, Y.S. Jin, T. Lu, Integrated, systems metabolic picture of acetone-butanol-ethanol fermentation by *Clostridium acetobutylicum*, Proc. Natl. Acad. Sci. U.S.A. 112 (2015) 8505–8510, https://doi.org/10.1073/pnas.1423143112.

[27] N. Qureshi, H.P. Blaschek, Butanol recovery from model solution/fermentation broth by pervaporation: evaluation of membrane performance, Biomass Bioenergy 17 (1999) 175–184, https://doi.org/10.1016/S0961-9534(99)00030-6.

[28] A.M. Zetty-Arenas, R.F. Alves, C.A.F. Portela, A.P. Mariano, T.O. Basso, L.P. Tovar, R. Maciel Filho, S. Freitas, Towards enhanced n-butanol production from sugarcane bagasse hemicellulosic hydrolysate: strain screening, and the effects of sugar concentration and butanol tolerance, Biomass Bioenergy 126 (2019) 190–198, https://doi.org/10.1016/j.biombioe.2019.05.011.

[29] H.I. Velázquez-Sánchez, R. Aguilar-López, Novel kinetic model for the simulation analysis of the butanol productivity of *Clostridium acetobutylicum ATCC 824* under different reactor configurations, Chin. J. Chem. Eng. 26 (2018) 812–821, https://doi.org/10.1016/j.cjche.2017.07.018.

[30] Q. Zhou, Y. Liu, W. Yuan, Kinetic modeling of lactic acid and acetic acid effects on butanol fermentation by *Clostridium saccharoperbutylacetonicum*, Fuel 226 (2018) 181–189, https://doi.org/10.1016/j.fuel.2018.04.019.

[31] Z. Dai, H. Dong, Y. Zhang, Y. Li, Elucidating the contributions of multiple aldehyde/alcohol dehydrogenases to butanol and ethanol production in *Clostridium acetobutylicum*, Sci. Rep. 6 (2016) 1–9, https://doi.org/10.1038/srep28189.

[32] A. da C. Gomes, M.I. Rodrigues, D. de França Passos, A. Machado de Castro, L. Maria Mello Santa Anna, N. Pereira, Acetone–butanol–ethanol fermentation from sugarcane bagasse hydrolysates: utilization of C5 and C6 sugars, Electron, J. Biotechnol. 42 (2019) 16–22, https://doi.org/10.1016/j.ejbt.2019.10.004.

[33] Y. Zhang, B. Han, T.C. Ezeji, Biotransformation of furfural and 5-hydroxymethyl furfural (HMF) by *Clostridium acetobutylicum ATCC 824* during butanol fermentation, N. Biotech. 29 (2012) 345–351, https://doi.org/10.1016/j.nbt.2011.09.001.

[34] N. Qureshi, M.J. Bowman, B.C. Saha, R. Hector, M.A. Berhow, M.A. Cotta, Effect of cellulosic sugar degradation products (furfural and hydroxymethyl furfural) on acetone-butanol-ethanol (ABE) fermentation using *Clostridium beijerinckii P260*, Food Bioprod. Process. 90 (2012) 533–540, https://doi.org/10.1016/j.fbp.2011.09.002.

[35] Y. Tashiro, K. Takeda, G. Kobayashi, K. Sonomoto, A. Ishizaki, S. Yoshino, High butanol production by *Clostridium saccharoperbutylacetonicum N1-4* in fed-batch culture with pH-stat continuous butyric acid and glucose feeding method, J. Biosci. Bioeng. 98 (2004) 263–268, https://doi.org/10.1263/jbb.98.263.

[36] C.M. Cooksley, Y. Zhang, H. Wang, S. Redl, K. Winzer, N.P. Minton, Targeted mutagenesis of the *Clostridium acetobutylicum* acetone-butanol-ethanol fermentation pathway, Metab. Eng. 14 (2012) 630–641, https://doi.org/10.1016/j.ymben.2012.09.001.

[37] X. Hou, W. Peng, L. Xiong, C. Huang, X. Chen, X. Chen, W. Zhang, Engineering *Clostridium acetobutylicum* for alcohol production, J. Biotechnol. 166 (2013) 25–33, https://doi.org/10.1016/j.jbiotec.2013.04.013.

[38] S.Y. Lee, Y.S. Jang, J.Y. Lee, J. Lee, J.H. Park, J.A. Im, M.H. Eom, J. Lee, S.H. Lee, H. Song, J.H. Cho, D.Y. Seung, Enhanced butanol production obtained by reinforcing the direct butanol-forming route in *Clostridium acetobutylicum*, mBio 3 (2012), https://doi.org/10.1128/mBio.00314-12.

[39] J. Votruba, B. Volesky, L. Yerushalmi, Mathematical model of a batch acetone–butanol fermentation, Biotechnol. Bioeng. 28 (1986) 247–255, https://doi.org/10.1002/bit.260280215.